Cell Reports

Premature Sister Chromatid Separation Is Poorly Detected by the Spindle Assembly Checkpoint as a Result of System-Level Feedback

Graphical Abstract

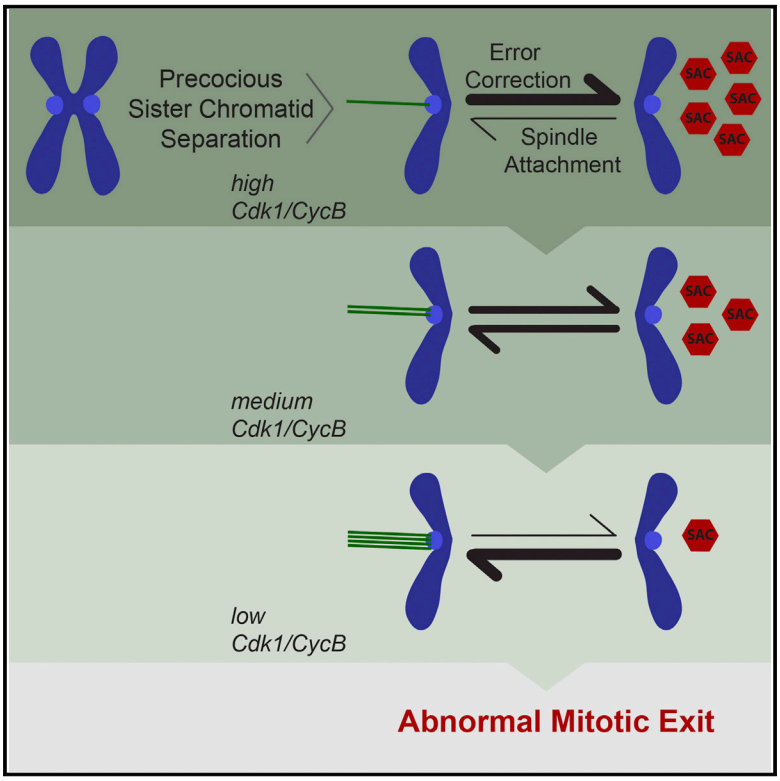

Highlights

- Precocious sister chromatid separation does not elicit robust SAC activation
- Error-correction efficiency declines gradually upon premature cohesion loss
- Mitotic exit in the absence of cohesin is accelerated by multiple feedback loops
- Cells with premature sister chromatid separation are ultrasensitive to Cdk1 inhibition

Authors

Mihailo Mirkovic, Lukas H. Hutter, Béla Novák, Raquel A. Oliveira

Correspondence

rcoliveira@igc.gulbenkian.pt

In Brief

Mirkovic et al. show that premature loss of sister chromatid cohesion during mitosis does not trigger a robust checkpoint response. Quantitative live-cell imaging and mathematical modeling approaches describe several feedback loops between the error-correction machinery, the spindle assembly checkpoint (SAC), and Cdk1 that compromise the efficient detection of cohesion defects.

Mirkovic et al., 2015, Cell Reports *13*, 469–478
October 20, 2015
http://dx.doi.org/10.1016/j.celrep.2015.09.020

Cell Reports
Report

Premature Sister Chromatid Separation Is Poorly Detected by the Spindle Assembly Checkpoint as a Result of System-Level Feedback

Mihailo Mirkovic,[1] Lukas H. Hutter,[2] Béla Novák,[2] and Raquel A. Oliveira[1,*]
[1]Instituto Gulbenkian de Ciência, Rua da Quinta Grande, 2780-156 Oeiras, Portugal
[2]Department of Biochemistry, Oxford Center for Integrative Systems Biology, University of Oxford, Oxford OX1 3QU, UK
*Correspondence: rcoliveira@igc.gulbenkian.pt
http://dx.doi.org/10.1016/j.celrep.2015.09.020

SUMMARY

Sister chromatid cohesion, mediated by the cohesin complex, is essential for faithful mitosis. Nevertheless, evidence suggests that the surveillance mechanism that governs mitotic fidelity, the spindle assembly checkpoint (SAC), is not robust enough to halt cell division when cohesion loss occurs prematurely. The mechanism behind this poor response is not properly understood. Using developing *Drosophila* brains, we show that full sister chromatid separation elicits a weak checkpoint response resulting in abnormal mitotic exit after a short delay. Quantitative live-cell imaging approaches combined with mathematical modeling indicate that weak SAC activation upon cohesion loss is caused by weak signal generation. This is further attenuated by several feedback loops in the mitotic signaling network. We propose that multiple feedback loops involving cyclin-dependent kinase 1 (Cdk1) gradually impair error-correction efficiency and accelerate mitotic exit upon premature loss of cohesion. Our findings explain how cohesion defects may escape SAC surveillance.

INTRODUCTION

Faithful chromosome segregation is governed by the spindle assembly checkpoint (SAC), a surveillance mechanism that senses spindle attachments and prevents progression through mitosis until all chromosomes are properly bioriented (Musacchio and Salmon, 2007). This checkpoint operates by generating a signal (the mitotic checkpoint complex [MCC]) that inhibits the anaphase-promoting complex/cyclosome (APC/C) and thereby anaphase onset (Musacchio and Salmon, 2007). Unattached kinetochores serve as a scaffold for the production of the MCC, but it has long been debated whether or not tension across sister chromatids (and/or intra-kinetochore tension) can also be sensed by this checkpoint (Khodjakov and Pines, 2010; Maresca and Salmon, 2010). Nevertheless, it is well accepted that tension plays a central role in SAC responsiveness, even if indirectly, by modulating spindle attachments (Khodjakov and Pines, 2010; Maresca and Salmon, 2010; Nezi and Musacchio, 2009; Pinsky and Biggins, 2005). This regulation is achieved by error-correction (EC) mechanisms, primarily mediated by Aurora B kinase (AurB), which destabilize kinetochore-microtubule (KT-MT) interactions that are not under tension (Carmena et al., 2012; Liu et al., 2009).

Sister chromatid cohesion, mediated by the cohesin complex (Nasmyth and Haering, 2009; Peters and Nishiyama, 2012), is a major contributor to the establishment of tension, as it provides the counterforce that resists microtubule pulling forces upon spindle attachment (Oliveira et al., 2010; Tanaka et al., 2000). Cohesin is therefore essential for faithful mitosis, as it promotes biorientation and thereby prevents random genome segregation. Upon premature sister chromatid separation (PSCS), avoidance of mitotic errors relies on the SAC's ability to respond to cohesion defects and efficiently inhibit mitotic exit. However, defects in cohesion are associated with aneuploidy, including some human disorders linked to cohesin malfunction (Barbero, 2011; Brooker and Berkowitz, 2014; Losada, 2014), implying that mitotic exit takes place despite PSCS. Moreover, studies in budding yeast and mammalian cells indicate that cells with unreplicated genomes or PSCS eventually exit mitosis (Michaelis et al., 1997; O'Connell et al., 2008). This conundrum raises the possibility that cohesion loss results in weak SAC activation despite the established role for sister chromatid cohesion as a major tension contributor. The molecular mechanisms behind this poor response, however, are not fully understood. Here, we report a quantitative analysis on the robustness of SAC activation during mitosis when sister chromatid separation occurs prematurely.

RESULTS

Premature Loss of Sister Chromatid Cohesion Does Not Elicit a Robust SAC Response

To determine the strength of SAC response to PSCS, we used a tool for acute removal of cohesin in *Drosophila melanogaster*, based on artificial cleavage of the cohesin protein Rad21 by an exogenous protease (tobacco etch virus [TEV]) (Oliveira et al., 2010; Pauli et al., 2008). We focused our analysis on developing larval brain neuroblasts (NBs), stem cells that give rise to the

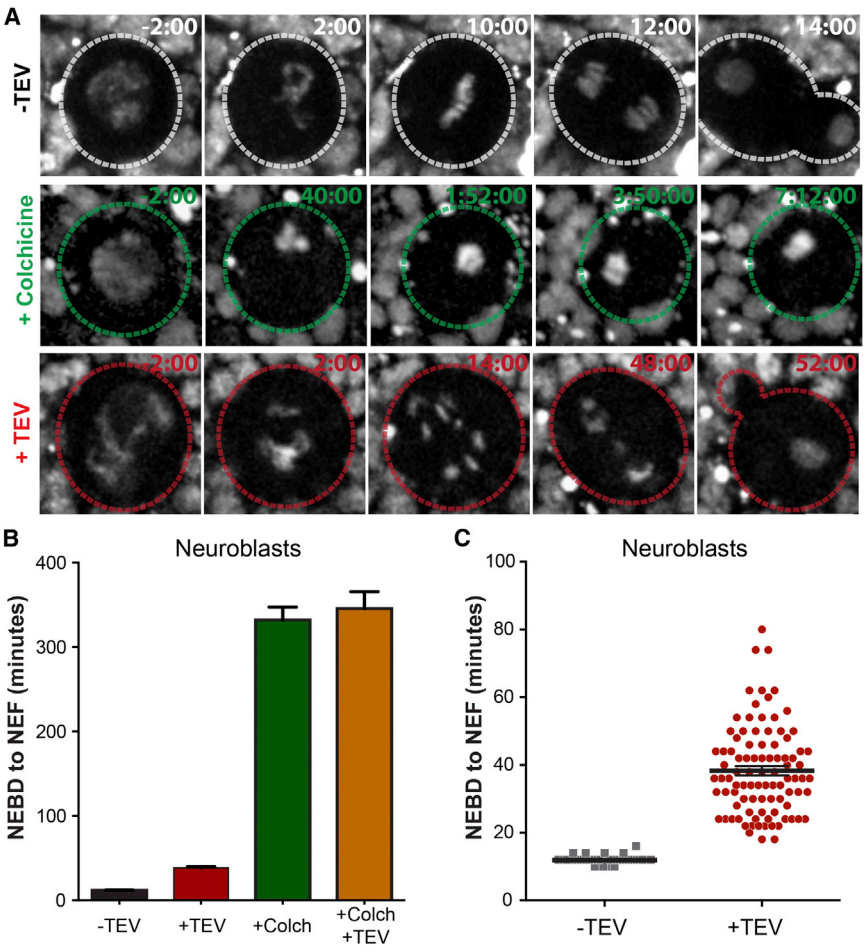

Figure 1. Premature Loss of Sister Chromatid Cohesion Induces a Short Mitotic Delay

(A) Images of dividing *Drosophila* neuroblasts from heat-shocked control strains (top), wild-type brains in 100 μM colchicine (middle), and strains surviving solely on $Rad21^{TEV}$ after TEV expression (bottom); strains express HisH2Av-mRFP1. Times (min:s) are relative to NEBD; scale bar, 5 μm.

(B) Average mitosis duration (NEBD to NEF) in heat-shocked control (n = 41, N = 4), TEV-mediated cohesin cleavage (n = 93, N = 8), colchicine-treated (n = 57, N = 6) and colchicine-treated after cohesin cleavage (n = 15, N = 2) larval neuroblasts (mean ± SEM).

(C) Mitosis duration (NEBD to NEF) in wild-type (heat-shock control) and TEV-mediated cohesin cleavage larval neuroblasts.

n, number of cells; N, number of brains. See also Figure S1 and Movies S1 and S2.

CNS. These cells arrest for many hours in mitosis when incubated with spindle poisons such as colchicine (Figures 1A and 1B). To induce cohesin cleavage, we used strains that contain solely TEV-sensitive cohesin complexes and express TEV protease under the heat-shock promoter (Pauli et al., 2008). Heat shock delays mitotic entry and nuclear division is resumed 148 ± 75 min (n = 113 cells, N = 14 brains analyzed) after heat shock, enabling analysis of cohesion loss within a single cell cycle (Figure S1). To evaluate the robustness of the SAC in the presence of PSCS, we quantified the time cells spend in mitosis (from nuclear envelope breakdown [NEBD] to nuclear envelope formation [NEF]). Whereas mitosis in control cells lasts ~12 min (with or without heat shock), TEV-mediated cohesin cleavage results in longer mitosis (38.3 ± 13.1 min) (Figures 1 and S1D; Movies S1 and S2). NBs from larvae not subjected to heat shock do not show any mitotic delay (Figure S1D). These results indicate that NBs elicit a SAC response that delays mitotic exit in response to PSCS. However, this arrest is relatively modest when compared to colchicine-induced arrest (Figure 1B). A similar response was observed in ganglion mother cells (GMCs), secondary precursor cells that derive from NBs (Figures S1E and S1F). Importantly, cohesin cleavage does not shorten the mitotic arrest in colchicine (Figure 1B), implying that cohesin depletion alone has no major effect on the SAC signaling capacity.

Loss of Sister Chromatid Cohesion Activates EC Mechanisms during Early Mitosis

Drosophila neuronal cells are therefore highly SAC competent in response to spindle poisons but fail to respond robustly to cohesion loss. Prematurely separated single chromatids can form transient attachments to the spindle, yet these attachments lack forces significant enough to oppose microtubule pulling forces and likely have a reduced ability to generate tension (both inter- and intrakinetochore tension). Transient attachments should therefore be destabilized by the EC machinery (Carmena et al., 2012; Liu et al., 2009), creating unattached kinetochores that provide a SAC signal sufficiently strong enough to prevent mitotic exit. In contrast, our findings imply that the EC machinery and the SAC respond inefficiently to PSCS. Recent evidence suggests that, upon depletion of cohesin subunits, AurB is not properly localized and shows reduced activity toward its targets (Carretero et al., 2013; Kleyman et al., 2014; Yamagishi et al., 2010). In accordance, AurB, as well as the related haspin-mediated chromatin mark (histone-H3T3 phosphorylation), is delocalized and specifically reduced in the centromere vicinity upon cohesin cleavage (Figure S2). However, two critical observations indicate that a malfunctioning error correction cannot fully explain the reduced SAC response. First, during the initial stages of the arrest, we observe high levels of chromosome motion with oscillatory movements between the poles (Figures 2 and S3; Movies S2 and S3). Quantitative analysis of chromosome movement, estimated from the displacement of centromere positions (see details in Supplemental Experimental Procedures), reveals a high degree of chromatid motion, as evidenced by the high frequency

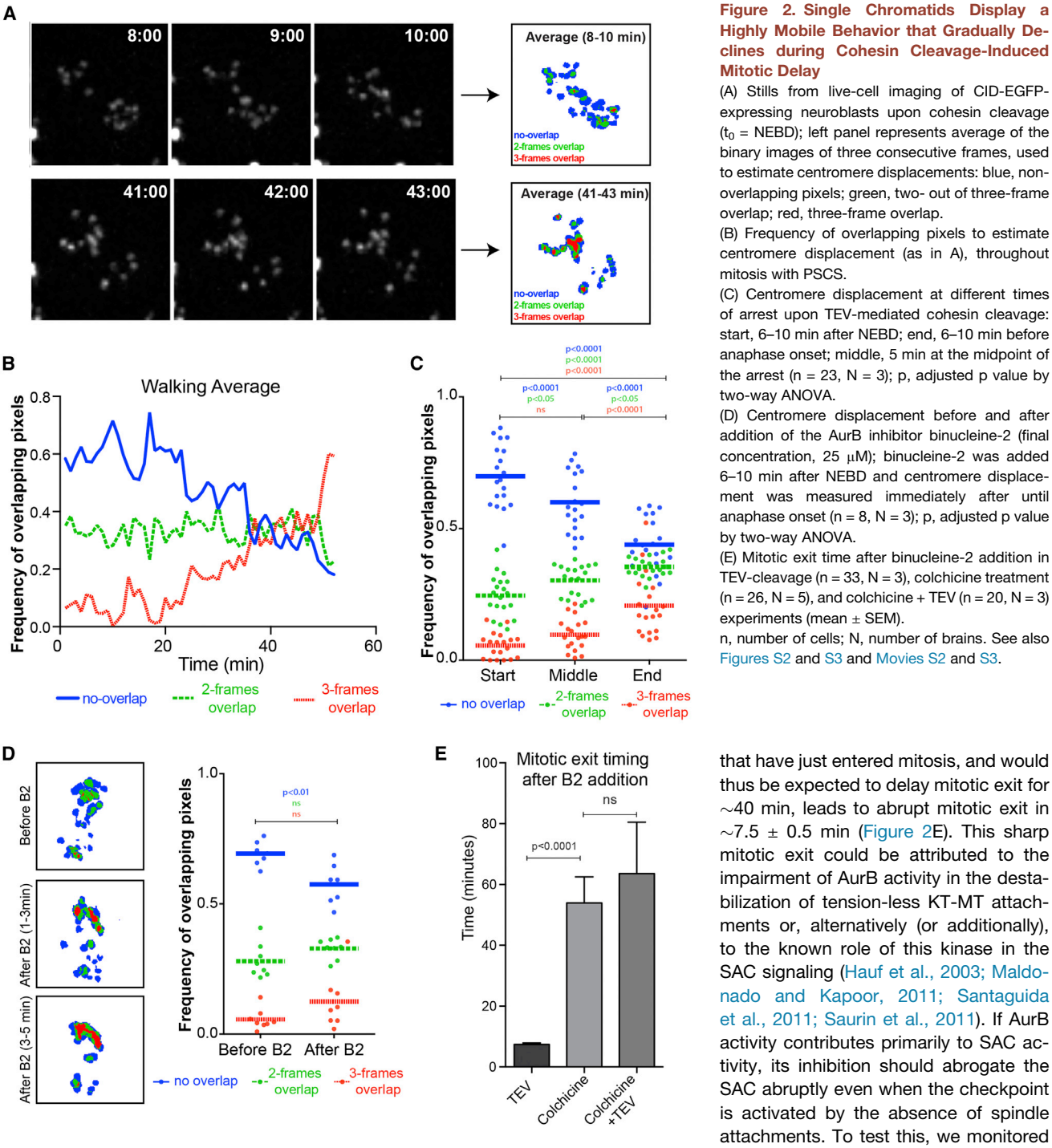

Figure 2. Single Chromatids Display a Highly Mobile Behavior that Gradually Declines during Cohesin Cleavage-Induced Mitotic Delay

(A) Stills from live-cell imaging of CID-EGFP-expressing neuroblasts upon cohesin cleavage (t_0 = NEBD); left panel represents average of the binary images of three consecutive frames, used to estimate centromere displacements: blue, non-overlapping pixels; green, two- out of three-frame overlap; red, three-frame overlap.

(B) Frequency of overlapping pixels to estimate centromere displacement (as in A), throughout mitosis with PSCS.

(C) Centromere displacement at different times of arrest upon TEV-mediated cohesin cleavage: start, 6–10 min after NEBD; end, 6–10 min before anaphase onset; middle, 5 min at the midpoint of the arrest (n = 23, N = 3); p, adjusted p value by two-way ANOVA.

(D) Centromere displacement before and after addition of the AurB inhibitor binucleine-2 (final concentration, 25 μM); binucleine-2 was added 6–10 min after NEBD and centromere displacement was measured immediately after until anaphase onset (n = 8, N = 3); p, adjusted p value by two-way ANOVA.

(E) Mitotic exit time after binucleine-2 addition in TEV-cleavage (n = 33, N = 3), colchicine treatment (n = 26, N = 5), and colchicine + TEV (n = 20, N = 3) experiments (mean ± SEM).

n, number of cells; N, number of brains. See also Figures S2 and S3 and Movies S2 and S3.

of non-overlapping centromere positions between consecutive frames (Figures 2A–2C). Such movements likely result from consecutive cycles of chromosome attachment, which are subsequently detached due to their low-tension state. Accordingly, movements are strongly reduced when AurB is inhibited by a specific inhibitor (binucleine-2) (Figure 2D). Second, the short but noticeable SAC response observed after cohesin cleavage depends on AurB activity. The addition of binucleine-2 to cells that have just entered mitosis, and would thus be expected to delay mitotic exit for ~40 min, leads to abrupt mitotic exit in ~7.5 ± 0.5 min (Figure 2E). This sharp mitotic exit could be attributed to the impairment of AurB activity in the destabilization of tension-less KT-MT attachments or, alternatively (or additionally), to the known role of this kinase in the SAC signaling (Hauf et al., 2003; Maldonado and Kapoor, 2011; Santaguida et al., 2011; Saurin et al., 2011). If AurB activity contributes primarily to SAC activity, its inhibition should abrogate the SAC abruptly even when the checkpoint is activated by the absence of spindle attachments. To test this, we monitored the time of mitotic exit upon binucleine-2 addition to colchicine-arrested cells, revealing that NBs eventually exit mitosis but take longer to do so, regardless of whether cohesin has been cleaved or not (Figure 2E). These results suggest that reversion of AurB-mediated phosphorylation events required for SAC maintenance is kinetically slow. We therefore favor that the sudden mitotic exit observed upon AurB inhibition in cohesin cleavage experiments results primarily from the inhibition of EC activity.

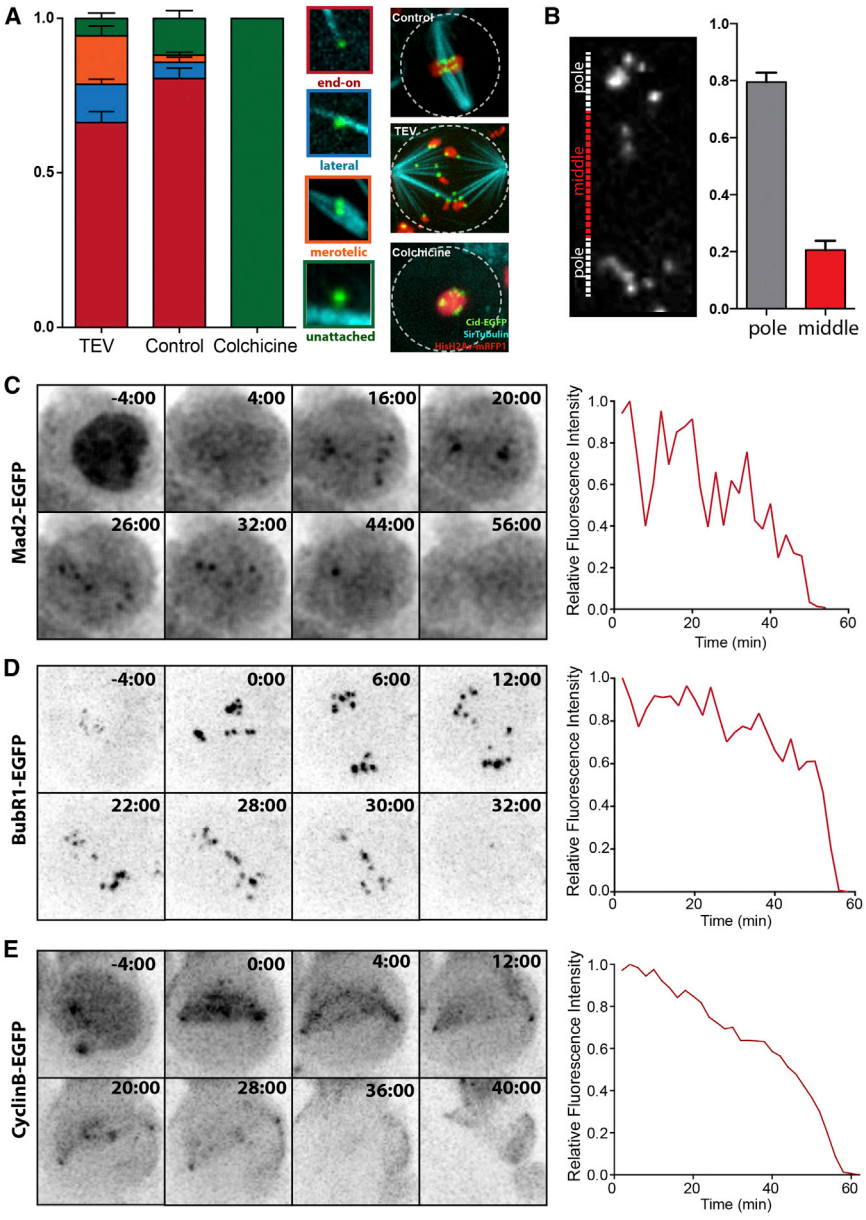

Figure 3. High Frequency of End-on Attachments Leads to Low Production of MCC and Premature Decay of Cyclin B

(A) Frequency of kinetochore attachment observed upon after cohesin cleavage; brains expressing HisH2Av-mRFP1 (red) and Cid-EGDP (green) were shortly incubated with 1:10,000 Sir-Tub probes (cyan) before brain squash. Graph shows average attachment profile for control (prometaphase and metaphase cells), cohesin-cleaved, and colchicine-treated NBs (n > 25 NBs, N = 3; mean ± SEM).

(B) Centromere distribution at the time of mitotic exit in cohesin cleaved NBs. For each image, the segregation plane, determined based on the two most distal centromeres, was divided into two equally sized regions as exemplified (n = 20, N = 4; mean ± SEM).

(C–E) Stills from live-cell imaging of Mad2-GFP (C), BubR1-GFP (D), and CycB-GFP (E) during the mitotic delay induced by cohesin cleavage. Times (min:s) are relative to NEBD; scale bars, 5 μm. Graphs represent the relative fluorescence intensity in cohesin cleavage, normalized to the maximum value within each dataset.

n, number of cells; N, number of brains. See also Figure S4 and Movie S4.

Attachments of Single Chromatids to the Mitotic Spindle Are Progressively Stabilized

Taken together, these observations imply that AurB is at least partly functional in the absence of cohesin. If so, why does PSCS not elicit a robust mitotic arrest? Given that the SAC response in the absence of cohesion depends on the ability to generate unattached kinetochores, we have monitored KT-MT interactions throughout mitosis. We first analyzed the degree of chromosome movement at different times of the arrest, as mentioned above. While chromosomes are highly dynamic in the initial stages of the arrest, their movement becomes gradually reduced, suggesting KT-MT interactions are progressively stabilized over time (Figures 2A, 2B, and S3). We envisioned three different possibilities that could account for KT-MT attachment stabilization in the presence of single sisters. First, stable attachments could arise from the accumulation of merotelic attachments, as previously reported in mitosis with unreplicated genomes (MUGs) (O'Connell et al., 2008). Second, attachments could be stabilized by tension in the absence of sister chromatid cohesion (e.g., due to cytoplasmic drag). Lastly, attachments may be abnormally stabilized even in the absence of maximal tension.

To distinguish among these possibilities, we analyzed KT-MT attachments in more detail (Figures 3A and S4A). This analysis revealed that cells with PSCS show high microtubule occupancy at kinetochores. The most prevalent form of attachment (66%) displays kinetochores at the end of a well-defined kinetochore bundle (end-on attachment). Very few chromatids appear totally unattached (6%). These findings suggest that even in the absence of cohesion, attachments to the spindle are relatively frequent (Figure 3A). Importantly, the low proportion of merotelic attachments (16%; Figure 3A) suggests that accumulation of these abnormal attachments is not the major cause for the observed decrease in motion. To confirm that this is also the case at mitotic exit, we measured centromere positions at this stage, as merotelic attachments should place centromeres in the middle of the segregation plane. In fact, in some TEV-cleaved cells, we do find centromeres that lag behind the major chromatin mass (on average ~20%; Figure 3B) and display obvious stretching once mitotic exit takes place, consistent with being bound to

both poles. However, most kinetochores were found to be placed facing the poles and did not stretch during poleward movement, supporting end-on attachment (Figure 3B). These results indicate that unlike the previous results in MUG cells (O'Connell et al., 2008), cohesion depletion in *Drosophila* NBs leads to mitotic exit without major accumulation of merotelic attachments.

To confirm that KT-MT attachments are indeed stabilized, we monitored the levels of Mad2-EGFP, which labels unattached kinetochores (Buffin et al., 2005), in live cells. We observe that upon cohesin cleavage, kinetochores show significant levels of Mad2 after NEBD (maximal amount approximately one-third of the levels in colchicine; data not shown) but with highly variable amounts during the initial stages of the arrest (Figures 3C, S4B, and S4D). These fluctuations in Mad2 signal are consistent with individual kinetochores undergoing repetitive cycles of Mad2 accumulation (detachment) and removal (re-attachment), as also suggested by their highly dynamic behavior (Figure 2). In addition to these fluctuations, the Mad2-EGFP signal decreases over time and cells exit mitosis once (and only when) all chromosomes are devoid of Mad2. Additionally, quantitative analysis of BubR1, a MCC component that leaves the kinetochores only when sisters are under tension (Buffin et al., 2005; Logarinho et al., 2004), reveals that its levels are reduced (one-third of the levels in colchicine cells) but relatively constant throughout the arrest (Figures 3D, S4C, and S4E; data not shown). We therefore favor that the mostly end-on spindle attachments of single sisters are progressively stabilized, even without maximal tension.

Cyclin B Is Gradually Degraded during Cohesin Cleavage-Mediated Mitotic Arrest

The results above suggest that throughout the mitotic delay, there is a gradual transition between different stages: at first, KT-MT interactions are highly unstable, resulting in a SAC signal strong enough to prevent mitotic exit; subsequently, single chromatids display more stable attachments to the spindle and thus decreased inhibitory signal production. To understand the basis of this transition, we considered the possible dynamic changes across the mitotic network. In contrast to the classical "all or nothing" view of the SAC (Rieder et al., 1995), recent evidence supports a graded SAC activity (Collin et al., 2013; Dick and Gerlich, 2013), arguing that its inhibitory activity is proportional to signal strength. It is therefore conceivable that an initial weak SAC signaling (caused by a high residence time of unstable attachments) leads to a partial APC/C activation and consequent Cyclin B (CycB) decay. To test this hypothesis, we monitored CycB-GFP levels in different experimental conditions. In the presence of colchicine, CycB levels remain high over the period of 1.5 hr (Figure S4F). In contrast, mitosis after PSCS leads to a significant decay in CycB levels (Figures 3E and S4F). This is consistent with a graded SAC response predicting that low MCC levels result in weak APC/C inhibition, leading to partial CycB degradation.

Mathematical Modeling of Multiple Feedback across the Mitotic Network

Because Cdk1 and CycB are required for almost all aspects of mitosis, a decay in CycB levels is likely the major drive for mitotic exit. To distinguish between different possible dynamic networks, we adopted a mathematical modeling approach, which provides a quantitative framework for the description of accelerated mitotic exit observed upon PSCS (Figure 4). We centered this analysis on the EC module, characterized by the role of centromeric AurB complexes in destabilizing attached microtubule binding sites (MBS_as) at KTs (AurB $-|$ MBS_a). AurB action is attenuated by KT stretching (stretch $-|$ AurB), which, in turn, is enhanced by sister chromatid cohesion upon amphitelic attachment. We characterize KT tension by a stretch constant (S), which is set to 1 during normal progression and to a small value (0.2) when cohesin cleavage is induced. The choice for a small but non-zero stretch value was based on recent findings that intrakinetochore stretch contributes to SAC silencing (Maresca and Salmon, 2009, 2010; Nannas and Murray, 2014; Uchida et al., 2009), together with the fact that single sisters were often found attached to the spindle (Figure 3).

Cohesin plays a seemingly paradox role on the action and level of AurB at centromeres (Figures 4 and S5A). The increased stretch caused by sister chromatid cohesion reduces AurB activity toward its targets (MBS_a $\rightarrow$ stretch $-|$ AurB$-|$ MBS_a), creating a double-negative feedback loop at the heart of the EC module. On the other hand, cohesion potentiates EC by stabilization of AurB molecules at centromeres (Figure S2, (Carretero et al., 2013; Kleyman et al., 2014), captured by reduced dissociation constant of AurB in the model. The net products of the EC module are unattached kinetochores (MBS_u), which through the SAC module catalyze the assembly of the inhibitory signal (MCC) that prevents mitotic exit by inhibiting APC/C-dependent CycB degradation (Figures 4 and S5A). All of these reactions are shared by the three models presented below in order to capture the dynamics of our experimental observations upon cohesin cleavage.

In our basic model, SAC signaling is strictly downstream of the EC module by assuming a constitutive rate for the localization of AurB to the centromere (Figure 4A). The behavior of control cells is nicely recapitulated by carefully chosen set of parameters (see details in Supplemental Experimental Procedures), as in the presence of cohesin, tension lowers AurB activity to stabilize attachments and allow mitotic exit. However, the mitotic timing observed in cohesin cleavage experiments cannot be captured with a small stretch constant, a likely scenario in the absence of cohesin (Figure S5B provides an overview of the stretch parameter effect in all our models). The basic model predicts a stable mitotic arrest in the absence of sufficient tension, because the EC module remains active and generates unattached kinetochores, which produce MCC and block mitotic exit (note the persistent MCC levels and absence of APC/C activation in Figure 4A). For these reasons, we assumed that additional feedback loops accelerate mitotic exit in the presence of single sisters.

In the SAC-feedback model, we considered the role of Cdk1-CycB (D'Angiolella et al., 2003; Rattani et al., 2014; Vázquez-Novelle et al., 2014) and AurB (Hauf et al., 2003; Maldonado and Kapoor, 2011; Santaguida et al., 2011; Saurin et al., 2011) in MCC assembly (Figure 4B). Introduction of these feedback loops accelerates mitotic exit, allowing us to establish kinetic

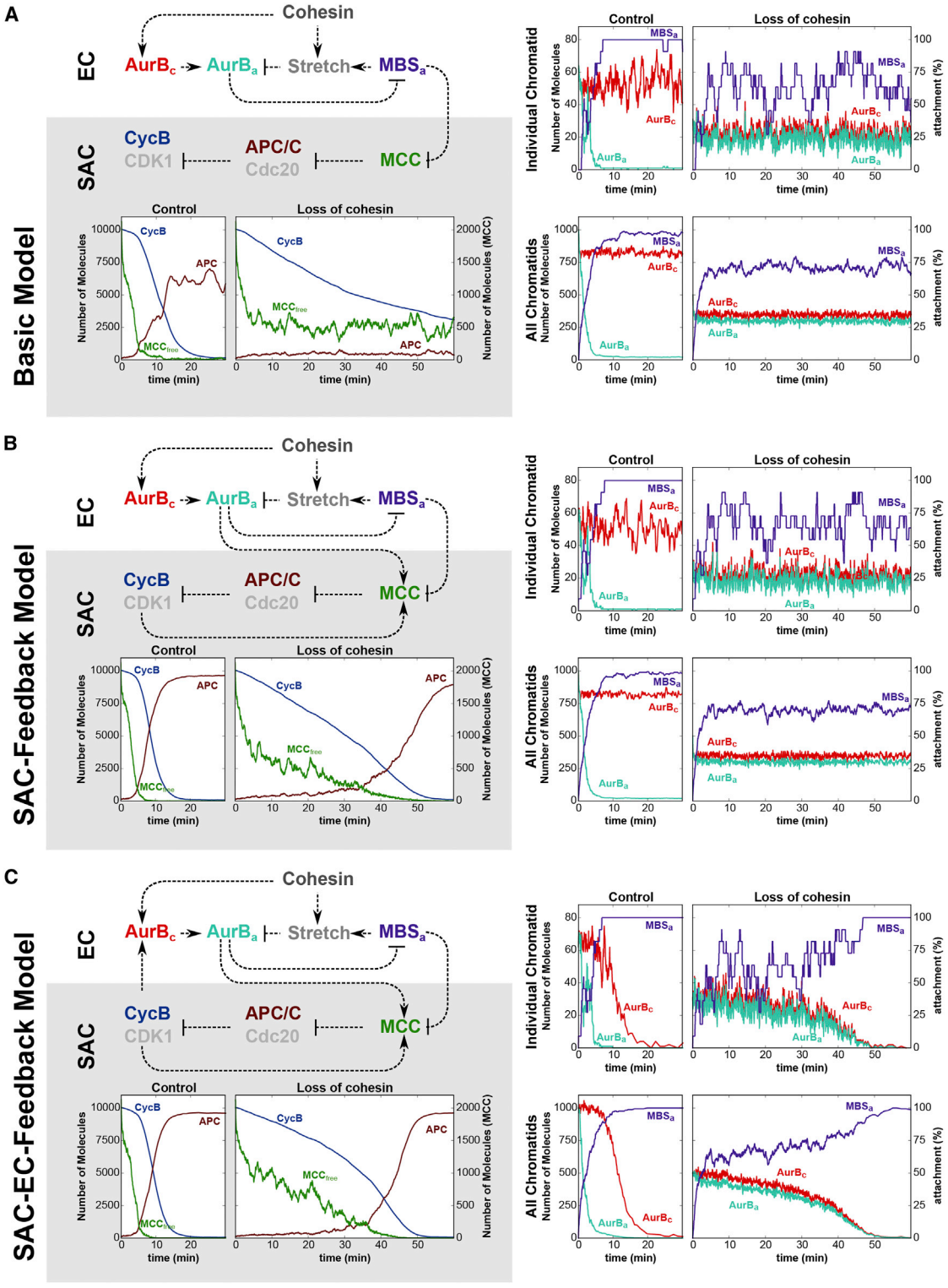

Figure 4. Mathematical Modeling of the Interplay between Error Correction and the Spindle Assembly Checkpoint

Three different scenarios for the interaction between the SAC and EC. Each panel shows a molecular influence diagram (top left), along with stochastic simulations for control and PSCS cells. Simulations show changes of key components of the EC and SAC modules over time (t_0 = NEBD). For the EC module, simulations depict the behavior of an individual chromatid (top) and all chromatids (bottom).

(legend continued on next page)

parameters that can fit the mitotic timing observed in both control and TEV-cleavage scenarios (Figure 4B and S5). However, this model predicts persistent stochastic fluctuations for the microtubule attachment profile (Figure 4B; note that MBS_as do not increase over time), which is inconsistent with our experimental observations (Figures 2 and 3). Additionally, this model postulates a slowing down in CycB degradation toward the later stages of the arrest (Figure 4B). In contrast, we observe that CycB degradation occurs in two stages: an initial linear decay followed by sharp degradation at the mitotic exit (Figure 3E; see rates of CycB degradation in Figure S5C).

For these reasons, an additional feedback loop was introduced by a positive effect of Cdk1-CycB on the EC machinery (SAC-EC-feedback model). Since Cdk1-CycB may affect EC by several mechanisms (e.g., AurB kinase activity/localization or microtubule dynamics), we simply described this effect by Cdk1-CycB dependence on centromeric AurB localization, as Cdk1 inactivation removes centromeric AurB at the metaphase-to-anaphase transition (Hümmer and Mayer, 2009; Mirchenko and Uhlmann, 2010; Pereira and Schiebel, 2003; Vázquez-Novelle and Petronczki, 2010). With the SAC-EC feedback in place, in silico simulations of the model fully recapitulate the mitotic progression observed upon PSCS (Figure 4C). In particular, inclusion of a positive feedback between SAC-EC makes the EC module sensitive to the levels of CycB. Consequently, simulations predict a gradual stabilization of KT-MT attachments, as seen experimentally (Figure 2). Additionally, this model postulates that CycB degradation occurs slowly during early stages of the arrest, followed by higher degradation rates at mitotic exit (Figure 3E; see also CycB-degradation rates in Figure S5C).

Cells with Premature Loss of Sister Chromatid Cohesion Are Ultrasensitive to Cdk1 Inhibition

Our experimental data are therefore best described by the SAC-EC-feedback model. Importantly, this model makes a critical testable prediction: mitosis duration upon cohesion depletion is ultrasensitive to mild Cdk1 inhibition. In contrast to a graded sensitivity scenario, in which mitotic timing would be proportional to the level of residual Cdk1 activity, our model postulates that the described feedback loops (SAC and EC feedback) will further accelerate mitotic exit in cells undergoing mitosis with PSCS. Consequently, mild Cdk1 inhibition is predicted to have a strong effect on mitosis duration in these cells (Figure 5A). Colchicine arrest also displays sensitivity to Cdk1 inhibition, although in this case to a lesser extent (note that in the absence of MT attachment, there is only one feedback [SAC feedback] potentiating sensitivity).

To test this prediction, we have first investigated the efficiency of different doses of Cdk inhibitor roscovitine in promoting mitotic exit in colchicine-arrested cells (Figures 5B and 5C). While addition of 100 μM roscovitine is sufficient to abolish the colchicine arrest, a tenth of this inhibitor dose (10 μM) does not promote significant mitotic exit within the tested time frame (2 hr) (Figures 5B and 5C). Importantly, control NBs incubated with 10 μM roscovitine are able to enter and progress through mitosis with normal timing (Figure 5D). In contrast, such mild inhibition caused a significant reduction in the mitotic timing of cells undergoing mitosis with PSCS (Figure 5D).

The shorter mitotic delay observed upon mild Cdk1 inhibition is postulated to arise from an increased accumulation of KT-MT attachments with concomitant SAC signaling decrease (lower MCC production rate) (Figure 5E). Accordingly, the number of Mad2 signals at kinetochores in TEV-cleaved NBs, upon mild Cdk1 inhibition (10 μM roscovitine), was drastically reduced when compared to DMSO controls (Figure 5F). These results indicate that mild Cdk inhibition is sufficient to stabilize KT-MT interactions and decrease SAC signaling, despite having no effect on either mitotic progression of control cells or reverting colchicine-induced arrest. Thus, cells with premature loss of sister chromatid cohesion are ultrasensitive to Cdk inhibition due to the multiple feedback loops across the mitotic network. This further suggests that among the many aspects of mitosis controlled by Cdk1, KT-MT attachment stability and SAC response are among the most sensitive ones.

DISCUSSION

Our analysis reveals that removal of a major tension contributor, such as sister chromatid cohesion, is insufficient for robust SAC activation. Such poor response can be attributed to two major findings. First, single chromatids attach to the spindle with a high residence time. This may be attributed to slow kinetics of the EC mechanisms suboptimal efficiency of the EC machinery (Figure S2; Carretero et al., 2013; Kleyman et al., 2014; Yamagishi et al., 2010), and/or the existence of additional forces (e.g. polar ejection forces) that stabilize KT-MT attachments of single chromatids (Drpic et al., 2015 [this issue of *Cell Reports*]). This, in turn, results in low MCC production. Second, low MCC levels lead to partial CycB degradation, which feeds back on EC and MCC generation, promoting further stabilization of KT-MT attachments and a decrease in MCC production.

The feedback loops described in the SAC-EC-feedback model depict an amplification (positive feedback) loop between

(A) Basic model. The EC module uses AurB activity (AurBa) to destabilize KT-MT attachments and thereby increases the frequency of attached microtubule-bindings sites (MBS_as); MBS_as become stretched and reduce the action of AurBa; cohesin influences both the activity of AurB and the stretch; MBS_as input into the SAC module and suppress the formation of mitotic checkpoint complexes (MCCs); MCC inhibition of APC/C-dependent CycB degradation regulates Cdk1 activity, which is the output of the SAC module.

(B) The SAC-feedback model is an extension of the basic model. An additional internal positive feedback loop within the SAC module via Cdk1 and AurB promotes the production of MCCs.

(C) The SAC-EC-feedback model is a further extension of the SAC-feedback model, where Cdk1 activity not only promotes MCC assembly but also promotes centromeric AurB localization. The mutual input-output relationship between EC and SAC creates a positive feedback (amplification) loop (EC → SAC →EC). See also Figure S5.

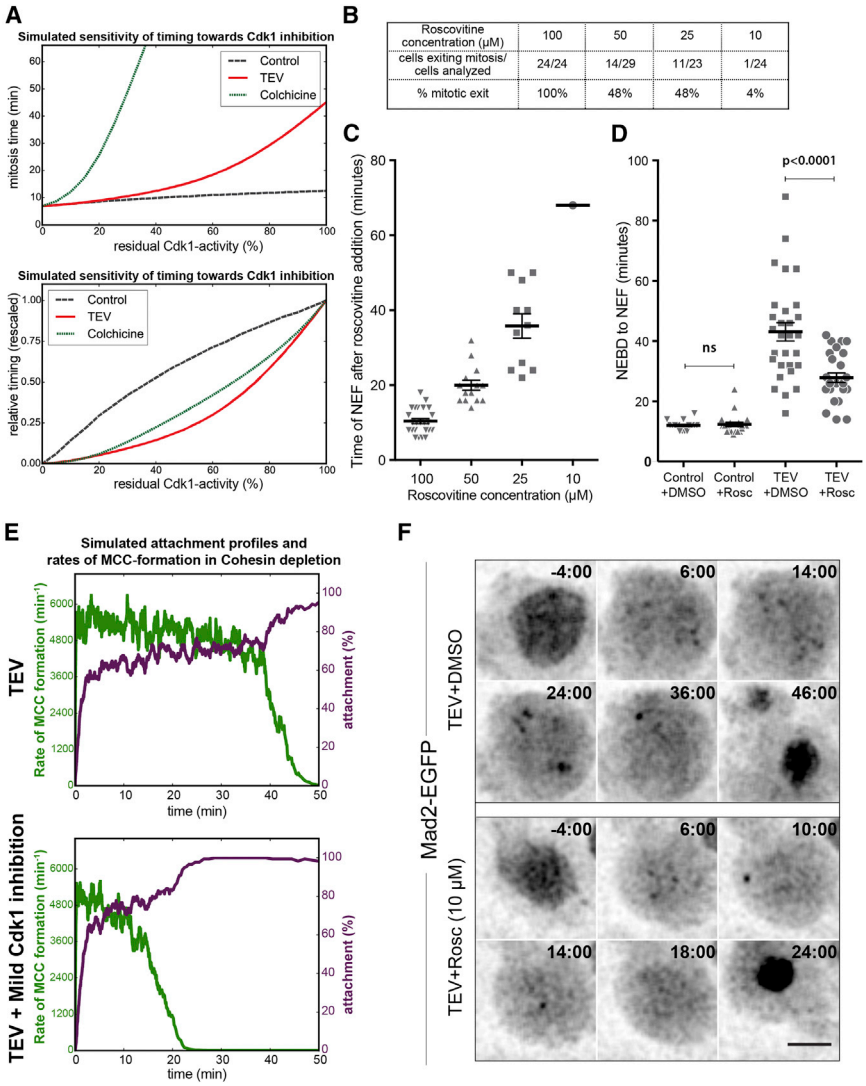

Figure 5. Mitosis with Precociously Separated Sister Chromatids Is Ultrasensitive to Cdk1 Inhibition

(A) Predicted sensitivity of control, TEV-, and colchicine-treated cells to Cdk1-inhibition. Mitotic exit timing was determined by the time when the CycB level is reduced to 10% of its initial value. Bottom panel shows relative sensitivity of the different treatments; mitotic durations were re-scaled between 0 (mitotic duration at 0% Cdk1-activity) and 1 (mitotic duration at 100% Cdk1 activity).

(B and C) Frequency (B) and time (C) of mitotic exit observed upon the addition of different doses of roscovitine to colchicine-arrested brains within 2 hr.

(D) Mitosis duration in wild-type and TEV-mediated cohesin cleavage larval neuroblasts, with and without prior incubation with 10 μM roscovitine; p, adjusted p value by one-way ANOVA.

(E) Comparison of simulated attachment profiles and rates of MCC formation for cohesin cleaved cells with full Cdk1 activity (top) and subjected to ~30% Cdk1 inhibition (bottom).

(F) Stills from live-cell imaging of Mad2-GFP during the mitotic delay induced by TEV-mediated cohesin cleavage with and without incubation with 10 μM roscovitine. Times are relative to NEBD; scale bar, 5 μm.

the EC and SAC modules (EC → SAC →EC) that in control cells stabilizes the high-Cdk1-activity mitotic state until biorientation is achieved. However, these feedback loops render premature cohesion loss almost insensitive to SAC surveillance. Additionally, the high sensitivity of EC and SAC to Cdk1 inhibition described here may facilitate their rapid inactivation during anaphase, where stable KT-MT attachments have to be maintained despite the sudden loss of cohesion (Kops, 2014; Oliveira and Nasmyth, 2010). The caveat of such sensitivity is that it compromises how PSCS is sensed by the mitotic checkpoint. The frail SAC response upon PSCS may result from a weak contribution of cohesion defects as a selective pressure throughout evolution.

Drosophila has a low number of chromosomes (eight), making it more prone to silence the SAC upon cohesin cleavage within a testable time frame. As such, loss of cohesion in mammalian cells may lead to a more prolonged SAC response, due to the higher number of signaling kinetochores (e.g., mouse embryos arrest for over 17 hr upon cohesin cleavage in mitosis; Tachibana-Konwalski et al., 2013). Nevertheless, the regulatory networks described here are highly conserved across species, predicting that mammalian cells with PSCS will likely eventually satisfy the SAC. Importantly, mild cohesion defects leading to partial levels of cohesion loss may be totally undetected by the SAC. This has important implications, as known cases of mitotic cohesion problems associated with human disease (e.g., Cornelia de Lange, Roberts, chronic atrial, and intestinal dysrhythmia [CIAD] syndromes) are indeed characterized by relatively mild levels of sister chromatid separation (Brooker and Berkowitz, 2014; Chetaille et al., 2014).

EXPERIMENTAL PROCEDURES

To destroy cohesin by TEV protease cleavage, *Drosophila* strains were used with TEV-cleavable Rad21 (Rad21^{TEV}) in a rad21-null background (*rad21*^{ex15}, *rad21*$^{550\text{-}3TEV}$*-myc*) (Pauli et al., 2008). TEV expression was induced by heat-shocking third-instar larvae at 37°C for 45 min. Brains from third-instar larvae were dissected and prepared for immunofluorescence or live-cell imaging as previously described (Oliveira et al., 2014). The mathematical models were first devised as systems of ordinary differential equations and simulated by Gillespie's stochastic simulation algorithm (SSA) after converting the rate of elementary reactions into propensity functions. Further details on experimental procedures can be found in Supplemental Experimental Procedures, including a complete list of genotypes used and details on tissue preparation, immunofluorescence, imaging acquisition, quantitative imaging analysis, model design, equations, and parameters.

SUPPLEMENTAL INFORMATION

Supplemental Information includes Supplemental Experimental Procedures, five figures, two tables, and four movies and can be found with this article online at http://dx.doi.org/10.1016/j.celrep.2015.09.020.

AUTHOR CONTRIBUTIONS

M.M. and R.A.O. designed the experiments; M.M. carried out the experiments. L.H.H. and B.N. performed the mathematical modelling. All authors wrote the paper.

ACKNOWLEDGMENTS

We would like to acknowledge the Cellular Imaging Unit (IGC) for help with microscopy; A. Tavares for excellent technical assistance; C. Sunkel and M. Carmena for antibodies; S. Heidmann, R. Karess, J. Raff, and the Bloomington Stock Center for fly strains; and L. Janssen, M. Bettencourt-Dias, and F. Janody for comments on the manuscript.

This work was supported by a PhD scholarship awarded to M.M. by the Fundação para a Ciência e Tecnologia (FCT), Portugal (SFRH/BD/52438/2013) and the Boehringer Ingelheim Fonds PhD fellowship program and EPSRC (to L.H.H.). The R.A.O. lab is supported by Marie Curie Career Integration Grant MCCIG321883/CCC and EMBO Installation Grant IG2778. The B.N. group is supported by EC FP7 (MitoSys/241548) and BBSRC sLoLa (BB/MM00354X/1).

Received: April 8, 2015
Revised: July 24, 2015
Accepted: September 8, 2015
Published: October 8, 2015

REFERENCES

Barbero, J.L. (2011). Sister chromatid cohesion control and aneuploidy. Cytogenet. Genome Res. *133*, 223–233.

Brooker, A.S., and Berkowitz, K.M. (2014). The roles of cohesins in mitosis, meiosis, and human health and disease. Methods Mol. Biol. *1170*, 229–266.

Buffin, E., Lefebvre, C., Huang, J., Gagou, M.E., and Karess, R.E. (2005). Recruitment of Mad2 to the kinetochore requires the Rod/Zw10 complex. Curr. Biol. *15*, 856–861.

Carmena, M., Wheelock, M., Funabiki, H., and Earnshaw, W.C. (2012). The chromosomal passenger complex (CPC): from easy rider to the godfather of mitosis. Nat. Rev. Mol. Cell Biol. *13*, 789–803.

Carretero, M., Ruiz-Torres, M., Rodríguez-Corsino, M., Barthelemy, I., and Losada, A. (2013). Pds5B is required for cohesion establishment and Aurora B accumulation at centromeres. EMBO J. *32*, 2938–2949.

Chetaille, P., Preuss, C., Burkhard, S., Côté, J.M., Houde, C., Castilloux, J., Piché, J., Gosset, N., Leclerc, S., Wünnemann, F., et al.; FORGE Canada Consortium (2014). Mutations in SGOL1 cause a novel cohesinopathy affecting heart and gut rhythm. Nat. Genet. *46*, 1245–1249.

Collin, P., Nashchekina, O., Walker, R., and Pines, J. (2013). The spindle assembly checkpoint works like a rheostat rather than a toggle switch. Nat. Cell Biol. *15*, 1378–1385.

D'Angiolella, V., Mari, C., Nocera, D., Rametti, L., and Grieco, D. (2003). The spindle checkpoint requires cyclin-dependent kinase activity. Genes Dev. *17*, 2520–2525.

Dick, A.E., and Gerlich, D.W. (2013). Kinetic framework of spindle assembly checkpoint signalling. Nat. Cell Biol. *15*, 1370–1377.

Drpic, D., Pereira, A.J., Barisic, M., Maresca, T.J., and Maiato, H. (2015). Polar ejection forces promote the conversion from lateral to end-on kinetochore-microtubule attachments on mono-oriented chromosomes. Cell Rep. *13*, this issue, 460–468.

Hauf, S., Cole, R.W., LaTerra, S., Zimmer, C., Schnapp, G., Walter, R., Heckel, A., van Meel, J., Rieder, C.L., and Peters, J.M. (2003). The small molecule Hesperadin reveals a role for Aurora B in correcting kinetochore-microtubule attachment and in maintaining the spindle assembly checkpoint. J. Cell Biol. *161*, 281–294.

Hümmer, S., and Mayer, T.U. (2009). Cdk1 negatively regulates midzone localization of the mitotic kinesin Mklp2 and the chromosomal passenger complex. Curr. Biol. *19*, 607–612.

Khodjakov, A., and Pines, J. (2010). Centromere tension: a divisive issue. Nat. Cell Biol. *12*, 919–923.

Kleyman, M., Kabeche, L., and Compton, D.A. (2014). STAG2 promotes error correction in mitosis by regulating kinetochore-microtubule attachments. J. Cell Sci. *127*, 4225–4233.

Kops, G.J. (2014). Cell division: SACing the anaphase problem. Curr. Biol. *24*, R224–R226.

Liu, D., Vader, G., Vromans, M.J., Lampson, M.A., and Lens, S.M. (2009). Sensing chromosome bi-orientation by spatial separation of aurora B kinase from kinetochore substrates. Science *323*, 1350–1353.

Logarinho, E., Bousbaa, H., Dias, J.M., Lopes, C., Amorim, I., Antunes-Martins, A., and Sunkel, C.E. (2004). Different spindle checkpoint proteins monitor microtubule attachment and tension at kinetochores in Drosophila cells. J. Cell Sci. *117*, 1757–1771.

Losada, A. (2014). Cohesin in cancer: chromosome segregation and beyond. Nat. Rev. Cancer *14*, 389–393.

Maldonado, M., and Kapoor, T.M. (2011). Constitutive Mad1 targeting to kinetochores uncouples checkpoint signalling from chromosome biorientation. Nat. Cell Biol. *13*, 475–482.

Maresca, T.J., and Salmon, E.D. (2009). Intrakinetochore stretch is associated with changes in kinetochore phosphorylation and spindle assembly checkpoint activity. J. Cell Biol. *184*, 373–381.

Maresca, T.J., and Salmon, E.D. (2010). Welcome to a new kind of tension: translating kinetochore mechanics into a wait-anaphase signal. J. Cell Sci. *123*, 825–835.

Michaelis, C., Ciosk, R., and Nasmyth, K. (1997). Cohesins: chromosomal proteins that prevent premature separation of sister chromatids. Cell *91*, 35–45.

Mirchenko, L., and Uhlmann, F. (2010). Sli15(INCENP) dephosphorylation prevents mitotic checkpoint reengagement due to loss of tension at anaphase onset. Curr. Biol. *20*, 1396–1401.

Musacchio, A., and Salmon, E.D. (2007). The spindle-assembly checkpoint in space and time. Nat. Rev. Mol. Cell Biol. *8*, 379–393.

Nannas, N.J., and Murray, A.W. (2014). Tethering sister centromeres to each other suggests the spindle checkpoint detects stretch within the kinetochore. PLoS Genet. *10*, e1004492.

Nasmyth, K., and Haering, C.H. (2009). Cohesin: its roles and mechanisms. Annu. Rev. Genet. *43*, 525–558.

Nezi, L., and Musacchio, A. (2009). Sister chromatid tension and the spindle assembly checkpoint. Curr. Opin. Cell Biol. *21*, 785–795.

O'Connell, C.B., Loncarek, J., Hergert, P., Kourtidis, A., Conklin, D.S., and Khodjakov, A. (2008). The spindle assembly checkpoint is satisfied in the absence of interkinetochore tension during mitosis with unreplicated genomes. J. Cell Biol. *183*, 29–36.

Oliveira, R.A., and Nasmyth, K. (2010). Getting through anaphase: splitting the sisters and beyond. Biochem. Soc. Trans. *38*, 1639–1644.

Oliveira, R.A., Hamilton, R.S., Pauli, A., Davis, I., and Nasmyth, K. (2010). Cohesin cleavage and Cdk inhibition trigger formation of daughter nuclei. Nat. Cell Biol. *12*, 185–192.

Oliveira, R.A., Kotadia, S., Tavares, A., Mirkovic, M., Bowlin, K., Eichinger, C.S., Nasmyth, K., and Sullivan, W. (2014). Centromere-independent accumulation of cohesin at ectopic heterochromatin sites induces chromosome stretching during anaphase. PLoS Biol. *12*, e1001962.

Pauli, A., Althoff, F., Oliveira, R.A., Heidmann, S., Schuldiner, O., Lehner, C.F., Dickson, B.J., and Nasmyth, K. (2008). Cell-type-specific TEV protease cleavage reveals cohesin functions in Drosophila neurons. Dev. Cell *14*, 239–251.

Pereira, G., and Schiebel, E. (2003). Separase regulates INCENP-Aurora B anaphase spindle function through Cdc14. Science *302*, 2120–2124.

Peters, J.M., and Nishiyama, T. (2012). Sister chromatid cohesion. Cold Spring Harb. Perspect. Biol. *4*, 4.

Pinsky, B.A., and Biggins, S. (2005). The spindle checkpoint: tension versus attachment. Trends Cell Biol. *15*, 486–493.

Rattani, A., Vinod, P.K., Godwin, J., Tachibana-Konwalski, K., Wolna, M., Malumbres, M., Novák, B., and Nasmyth, K. (2014). Dependency of the spindle assembly checkpoint on Cdk1 renders the anaphase transition irreversible. Curr. Biol. *24*, 630–637.

Rieder, C.L., Cole, R.W., Khodjakov, A., and Sluder, G. (1995). The checkpoint delaying anaphase in response to chromosome monoorientation is mediated by an inhibitory signal produced by unattached kinetochores. J. Cell Biol. *130*, 941–948.

Santaguida, S., Vernieri, C., Villa, F., Ciliberto, A., and Musacchio, A. (2011). Evidence that Aurora B is implicated in spindle checkpoint signalling independently of error correction. EMBO J. *30*, 1508–1519.

Saurin, A.T., van der Waal, M.S., Medema, R.H., Lens, S.M., and Kops, G.J. (2011). Aurora B potentiates Mps1 activation to ensure rapid checkpoint establishment at the onset of mitosis. Nat. Commun. *2*, 316.

Tachibana-Konwalski, K., Godwin, J., Borsos, M., Rattani, A., Adams, D.J., and Nasmyth, K. (2013). Spindle assembly checkpoint of oocytes depends on a kinetochore structure determined by cohesin in meiosis I. Curr. Biol. *23*, 2534–2539.

Tanaka, T., Fuchs, J., Loidl, J., and Nasmyth, K. (2000). Cohesin ensures bipolar attachment of microtubules to sister centromeres and resists their precocious separation. Nat. Cell Biol. *2*, 492–499.

Uchida, K.S., Takagaki, K., Kumada, K., Hirayama, Y., Noda, T., and Hirota, T. (2009). Kinetochore stretching inactivates the spindle assembly checkpoint. J. Cell Biol. *184*, 383–390.

Vázquez-Novelle, M.D., and Petronczki, M. (2010). Relocation of the chromosomal passenger complex prevents mitotic checkpoint engagement at anaphase. Curr. Biol. *20*, 1402–1407.

Vázquez-Novelle, M.D., Sansregret, L., Dick, A.E., Smith, C.A., McAinsh, A.D., Gerlich, D.W., and Petronczki, M. (2014). Cdk1 inactivation terminates mitotic checkpoint surveillance and stabilizes kinetochore attachments in anaphase. Curr. Biol. *24*, 638–645.

Yamagishi, Y., Honda, T., Tanno, Y., and Watanabe, Y. (2010). Two histone marks establish the inner centromere and chromosome bi-orientation. Science *330*, 239–243.

Cell Reports

Supplemental Information

Premature Sister Chromatid Separation Is Poorly Detected by the Spindle Assembly Checkpoint as a Result of System-Level Feedback

Mihailo Mirkovic, Lukas H. Hutter, Béla Novák, and Raquel A. Oliveira

Figure S1

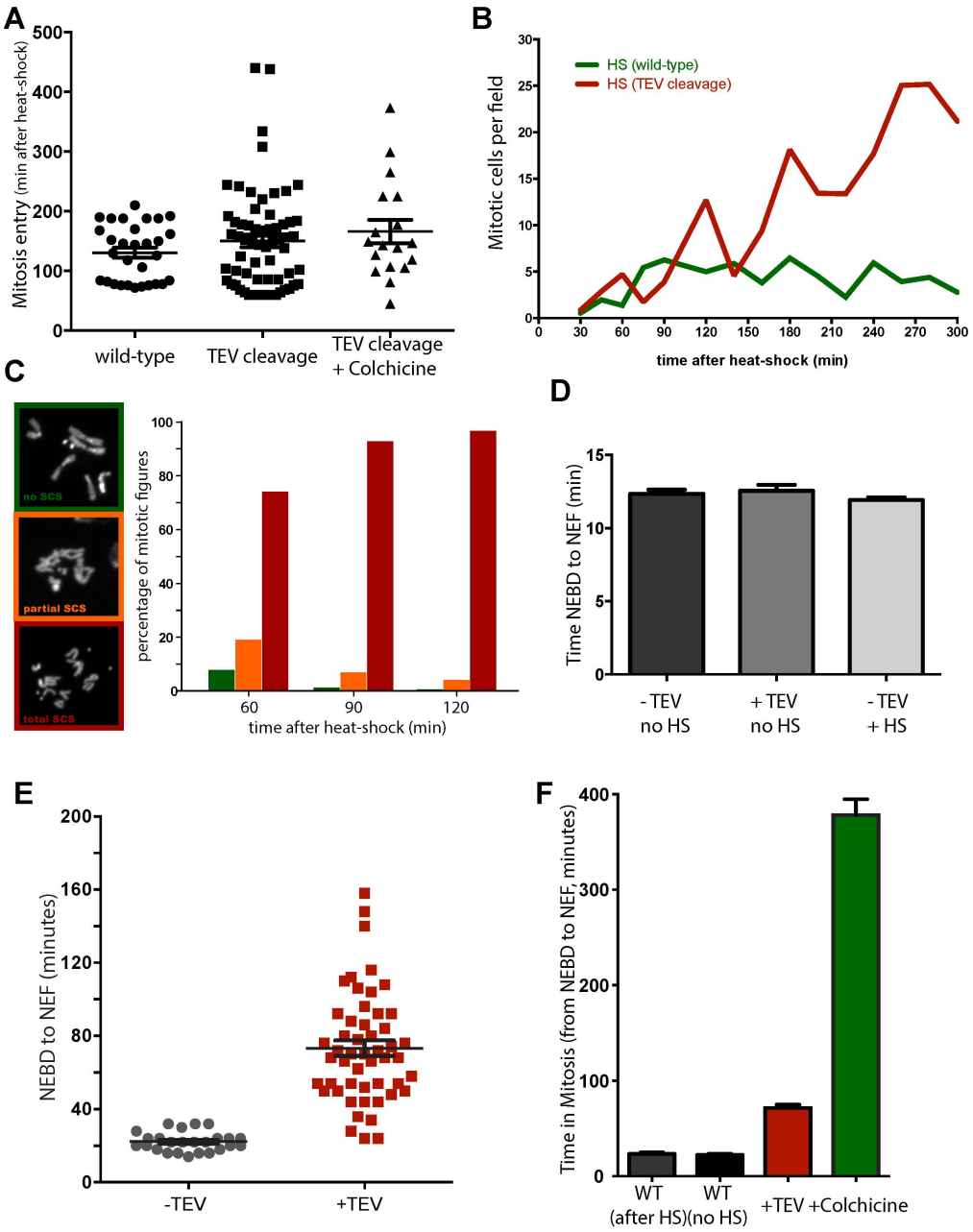

Figure S1, related to Figure 1 – TEV-mediated cleavage of cohesin allows analysis of the consequences of precocious sister chromatid cohesion separation within a single cell cycle. A) Time of entry into mitosis after heat-shock in the indicated experimental conditions showing that mitosis is not observed within the first 60 min after heat-shock, after which NBs asynchronously resume nuclear division. Note that TEV expression, cohesin cleavage or colchicine treatment, have no effect in the time of mitotic entry after heat-shock. **B)** Mitotic index in wild-type and cohesin-cleavage brains monitored in fixed samples at different times after heat-shock induced TEV expression; data points represent average number of mitotic figures (PH3 positive) per field. **C)** Quantification of precocious sister chromatid separation observed at different times after heat-shock-induced TEV protease expression, determined on acetic acid brain spreads (n=600 N=12 per time point, for each experimental condition); **D)** Time of mitosis (from NEBD to NEF) in the control without heatshock (n=62 N=6), control after heat-shock (n=41 N=4), and strains carrying the hsTEV transgene without heatshock (n=51 N=4), showing that neither heat-shock treatment nor leaky TEV expression influence progression through mitosis. **E)** Mitosis duration (NEBD to NEF) in heat-shocked wild-type and cohesin cleavage larval Ganglion Mother Cells (GMCs); **F)** Average mitosis duration (NEBD to NEF) in wild-type (n=20 N=3), wild-type after heat-shock, (n=25 N=3), cohesin cleaved (n=54 N=8), and colchicine treated (n=30 N=3) larval GMCs represented as mean ± SEM;

Figure S2

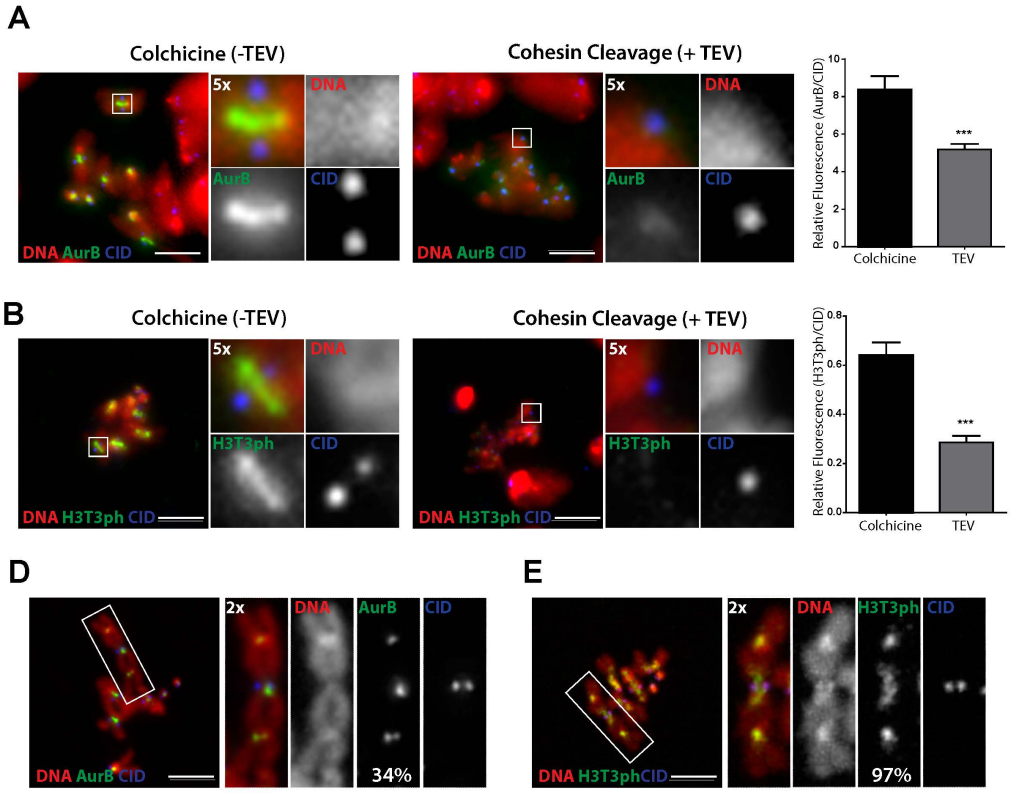

Figure S2, related to Figure 2 - Cohesin cleavage impairs proper centromeric localization of Aurora B. Spreads from larval brains from wild-type and cohesin cleaved strains immunostained for Aurora B **(A)** and H3T3ph **(B).** DNA is shown in red and CID in blue. Right graph depicts relative fluorescence intensity in the centromere vicinity in each experimental condition. **C)** Spreads from larval brains from C(2)EN strains immunostained for Aurora B (left) and H3T3ph (right) demonstrating their localization at ectopic heterochromatin sites, despite the absence of a proximal centromere (labelled with CID in blue). Numbers indicate the percentage of ectopic sites containing Aurora B / phH3T3. Scale bars are 5 µm.

Figure S3

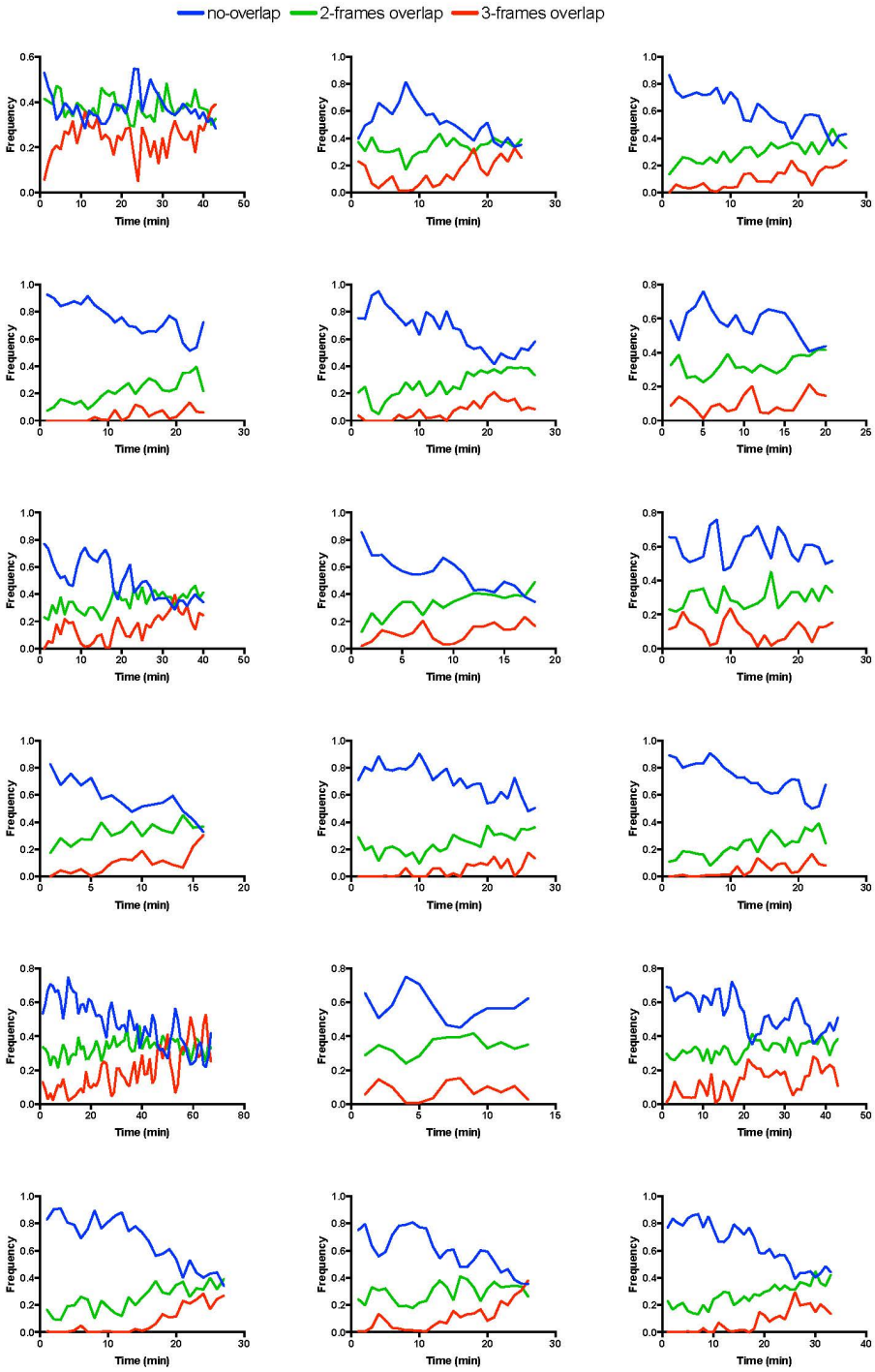

Figure S3, related to Figure 2 – Single chromatid movement decays gradually during mitotic delay induced by premature cohesin cleavage. Profile for chromatid movement observed in 18 individual cells after cohesin cleavage. Chromosome movement was measured from the displacement of individual centromeres within 3 consecutive frames, 6 min post-NEBD to anaphase onset; graphs represent frequency of overlapping pixels throughout the arrest. Blue represents non-overlapping pixels (fast movement), green represents pixels that overlap in 2 out of 3 frames (slow movement) and red represents pixels overlapping in the 3 frames (no movement). See also Movie S5.

Figure S4

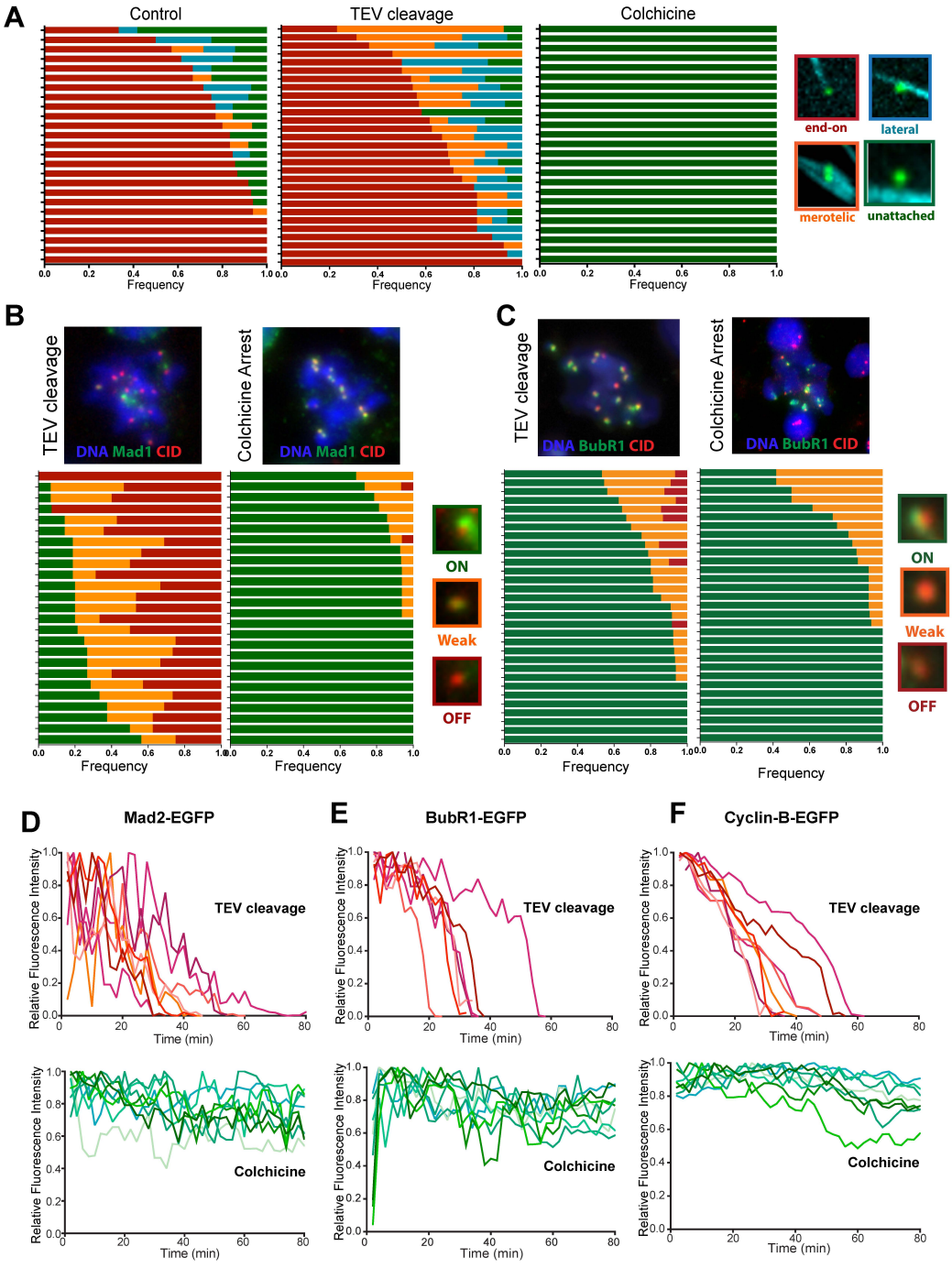

Figure S4, related to Figure 3 – Chromosome Attachment and localization of SAC components in single chromatids during mitotic arrest. A) Frequency of kinetochore attachment observed in controls (left), upon after cohesin cleavage (center) and after colchicine incubation (right); brains expressing HisH2Av-mRFP1 (red) and Cid-EGDP (green) were shortly incubated with 1:10.000 Sir-Tubulin probes (Cyan) before brain squash; each line in the graph represents the profile of a single cell (>25 NBs (N=3) for each experimental condition); **B and C)** Spreads from larval brains from colchicine-arrested and cohesin cleaved cells immunostained for Mad1 **(B)** and BubR1 **(C)** (in green). DNA is shown in blue and CID in red. Graph depicts relative frequency of kinetochores containing no, low, and high levels of Mad1/BubR1. Note that in contrast to colchicine-arrest, cohesin cleavage leads to reduced levels of Mad1 at kinetochores and a high asynchrony between the different analyzed cells (each at random points of the arrest). In contrast, BubR1 is mostly present at significant levels in all kinetochores of the analyzed cells. **(D-F)** Relative fluorescence intensity of Mad2-GFP **(D)**, BubR1-GFP **(E)** and CyclinB-GFP **(F)** in cohesin cleavage (red) and colchicine arrested (green) cells, normalized to the maximum value within each dataset. Times are relative to NEBD;

Figure S5

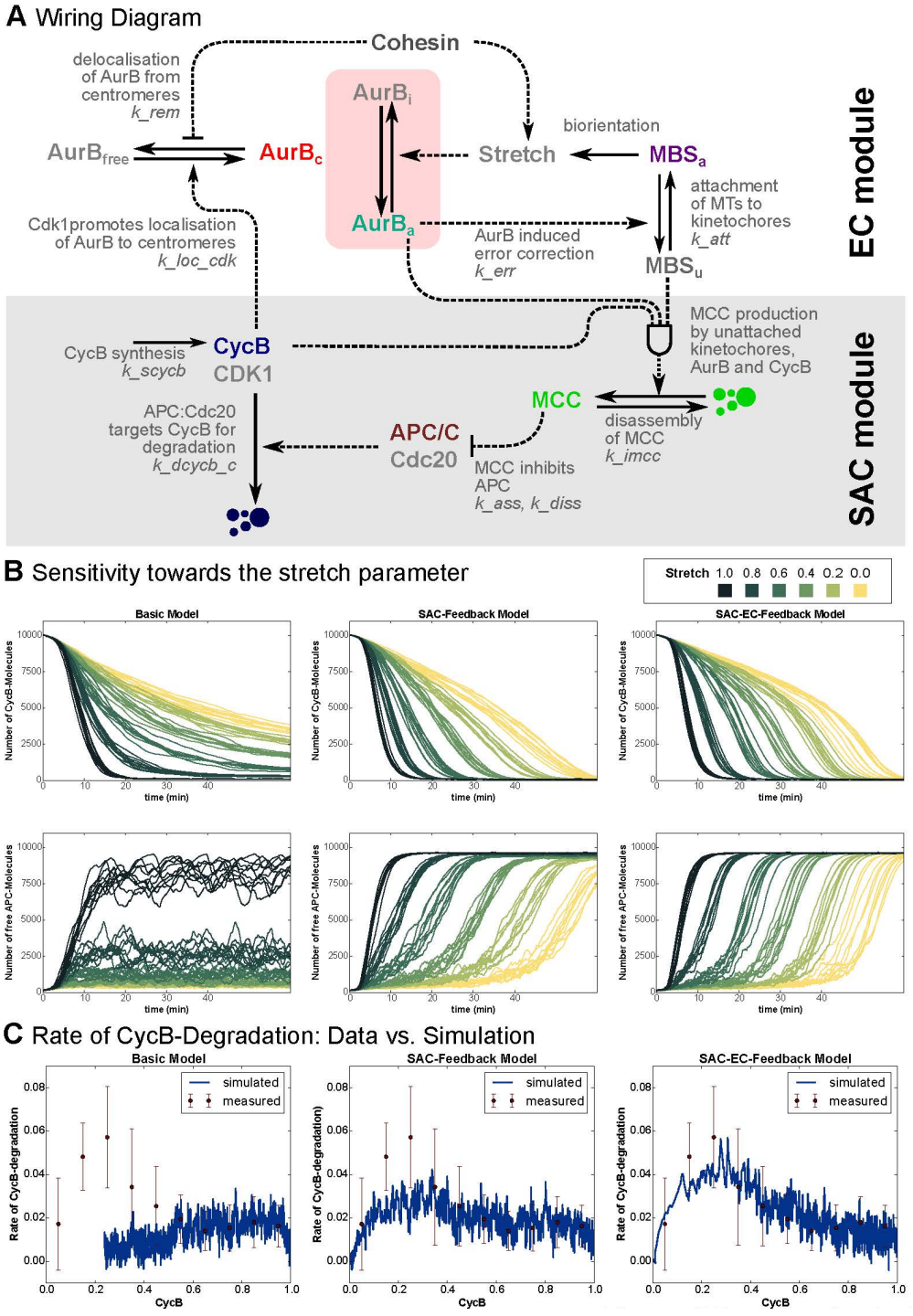

Figure S5, related to Figure 4 - Mathematical modelling of the interplay between error-correction (EC) and Spindle Assembly Checkpoint (SAC). A) Detailed molecular interaction network of EC and SAC: The EC module operates at centromeres/kinetochores and it uses Aurora-B activity to destabilize MT-KT attachments and thereby generates unattached MT-binding sites at KTs (MBSu) as an output of the EC module. Unattached MT binding sites of the KT signal to the SAC module by catalysing the production of Mitotic Checkpoint Complexes (MCC). MCC inhibition of APC/C-dependent CycB degradation regulates Cdk1 activity, which is the output of the SAC module. By promoting localization of AurB at centromeres, Cdk1 activity represents an input of EC. **B)** Numerical simulations of CycB (top row) and APC/C (bottom row) levels at different values of Stretch parameters in absence of cohesion with the three different models. **C)** Predicted rates of CycB-degradation after the loss of cohesins in the three model instances (blue lines) are plotted against degradation rates obtained from experimental data (red dots and error bars).

SUPPLEMENTAL MOVIES

Movie S1, related to Figure 1- Mitosis in a control neuroblast: Neuroblast undergoing mitosis after the heat shock. DNA is marked by H2AvD-mRFP1 (in red) centromere is marked by CID-GFP (in green). Times are relative to Nuclear Envelope Breakdown; scale bar equals 5 μm.

Movie S2, related to Figure 1 and 2- Nuclear division after cohesin cleavage: Neuroblast undergoing mitosis after cohesin has been cleaved prematurely by TEV; DNA is marked by H2AvD-mRFP1 (in red) centromere is marked by CID-GFP (in green); times are relative to Nuclear Envelope Breakdown). Note the dynamic behavior of centromeres upon premature cohesin cleavage; scale bar equals 5 μm.

Movie S3, related to Figure 2- Quantitative analysis of centromere motion after premature cohesin cleavage: Movies show walking average of the positions of centromeres (Cid-EGFP labelled) between 3 consecutive frames; Blue represents non-overlapping pixels, green represents pixels that overlap in 2 out of 3 frames and red represents pixels overlapping in the 3 frames. Movie shows 4 individual cells from 6 min-post NEBD until anaphase onset.

Movie S4, related to Figure 3- Kinetics of Mad2, BubR1 and Cyclin B upon cohesin cleavage: Time lapse imaging of Mad2-EGFP (left), BUBR1-GFP (middle), and Cyclin B-EGFP (right) in neuroblasts undergoing mitosis after cohesin cleavage by TEV protease. Times are relative to Nuclear Envelope Breakdown; scale bars are 5 μm.

SUPPLEMENTAL EXPERIMENTAL PROCEDURES

Fly strains:

To destroy cohesin by TEV protease cleavage, *Drosophila* strains were used with TEV-cleavable Rad21 ($Rad21^{TEV}$) in a Rad21-null background ($Rad21^{ex15}$, $Rad21^{550\text{-}3TEV}$-myc) (Pauli et al., 2008). TEV expression was induced by heat-shocking 3rd instar larvae at 37ºC for 45 minutes. After heat-shock, larvae were left to recover at room temperature. For live cell imaging, fly strains also expressed fluorescent markers as indicated in the tables below.

Table S1: List of Drosophila stocks used in this study.

Genotype	**Reference**
w-; +/+; Rad21^{ex15}, tubpr-Rad21$^{550\text{-}3TEV}$-myc *(4c)*	(Pauli et al., 2008)
w-; +/+; Rad21^{ex15}, poliubiq-His-RFP, tubpr-Rad21$^{550\text{-}3TEV}$ (4c)	(Oliveira et al., 2010)
w-; hspr-NLSv5TEV; Rad21^{ex3}/TM6B ubiGFP	(Pauli et al., 2008)
w-; HisH2AvD mRFP1 II.2; Cid-EGFP (CGC III.1)	(Schuh et al., 2007)
w-; HisH2AvD mRFP1 II.2 ; Rad21^{ex15}, tubpr-Rad21$^{550\text{-}3TEV}$(4c), CID-EGFP(CGC III.1)	(Oliveira et al., 2010)
w-; BubR1-GFP;+/+	(Buffin et al., 2005)
w- ; BubR1-GFP/CyO; Rad21^{ex15}, poliubiq-His-RFP, tubpr-Rad21$^{550\text{-}3TEV}$ (4c)	*This Study*
w- ; Mad2-GFP ; MKRS/TM6B	(Buffin et al., 2005)
w-; Mad2-GFP ; Rad21^{ex15}, poliubiq-His-RFP, tubpr-Rad21$^{550\text{-}3TEV}$(4c)	*This Study*
w-; poliubiq -CyclinB GFP	(Huang and Raff, 1999)
w-; poliubiq -CyclinB GFP ; Rad21^{ex15}, poliubiq-His-RFP, tubpr-Rad21 $^{550\text{-}3TEV}$(4c)	*This Study*
w+; C(2) EN;	(Novitski et al., 1981)

Table S2: List of specific genotypes used in this study.

Figure		**Label**	**Genotype**
1	A-C	-TEV	*w-; HisH2AvD mRFP1 II.2 ; Rad21^{ex15}, tubpr-Rad21$^{550\text{-}3TEV}$(4c), CID-EGFP(CGC III.1)*
		+TEV	*w-; hspr-NLSv5TEV/HisH2AvD-mRFP1 II.2; Rad21^{ex15}, tubpr-Rad21$^{550\text{-}3TEV}$*-myc *(4c), CID-EGFP-(CGCIII.1)/ Rad21^{ex3}*
		Colchicine	*w-; HisH2AvD mRFP1 II.2 ; Rad21^{ex15}, tubpr-Rad21$^{550\text{-}3TEV}$(4c), CID-EGFP(CGC III.1)*
2	A-E		*w-; hspr-NLSv5TEV/HisH2AvD-mRFP1 II.2; Rad21^{ex15}, tubpr-Rad21$^{550\text{-}3TEV}$*-myc *(4c), CID-EGFP-(CGCIII.1)/ Rad21^{ex3}*
3	A	Control	*w-; HisH2AvD mRFP1 II.2 ; Rad21^{ex15}, tubpr-Rad21$^{550\text{-}3TEV}$(4c), CID-EGFP(CGC III.1)*
		+ TEV	*w-; hspr-NLSv5TEV/HisH2AvD-mRFP1 II.2; Rad21^{ex15}, tubpr-Rad21$^{550\text{-}3TEV}$*-myc *(4c), CID-EGFP-(CGCIII.1)/ Rad21^{ex3}*
		Colchicine	*w-; HisH2AvD mRFP1 II.2 ; Rad21^{ex15}, tubpr-Rad21$^{550\text{-}3TEV}$(4c), CID-EGFP(CGC III.1)*
	B		*w-; hspr-NLSv5TEV/HisH2AvD-mRFP1 II.2; Rad21^{ex15}, tubpr-Rad21$^{550\text{-}3TEV}$*-myc *(4c), CID-EGFP-(CGCIII.1)/ Rad21^{ex3}*
	C	+TEV	*w-; hspr-NLSv5TEV/Mad2-EGFP; Rad21^{ex15}, poliubiq-His-RFP, tubpr-Rad21$^{550\text{-}3TEV}$(4c)/ Rad21^{ex3}*
	D	+TEV	*w-; hspr-NLSv5TEV/BubR1-EGFP; Rad21^{ex15}, poliubiq-His-RFP, tubpr-Rad21$^{550\text{-}3TEV}$(4c)/ Rad21^{ex3}*
	E	+TEV	*w-; hspr-NLSv5TEV/CycB-EGFP; Rad21^{ex15}, poliubiq-His-RFP, tubpr-Rad21$^{550\text{-}3TEV}$(4c)/ Rad21^{ex3}*
5	B, C		*w-; HisH2AvD mRFP1 II.2 ; Rad21^{ex15}, tubpr-Rad21$^{550\text{-}3TEV}$(4c), CID-EGFP(CGC III.1)*
	D	Control	*w-; HisH2AvD mRFP1 II.2 ; Rad21^{ex15}, tubpr-Rad21$^{550\text{-}3TEV}$(4c), CID-EGFP(CGC III.1)*
		+TEV	*w-; hspr-NLSv5TEV/Mad2-EGFP; Rad21^{ex15}, poliubiq-His-RFP, tubpr-Rad21$^{550\text{-}3TEV}$(4c)/ Rad21^{ex3}*
	F	+TEV	*w-; hspr-NLSv5TEV/Mad2-EGFP; Rad21^{ex15}, poliubiq-His-RFP, tubpr-Rad21$^{550\text{-}3TEV}$(4c)/ Rad21^{ex3}*
S1	A,D-F	-TEV	*w-; HisH2AvD mRFP1 II.2 ; Rad21^{ex15}, tubpr-Rad21$^{550\text{-}3TEV}$(4c), CID-EGFP(CGC III.1)*
		+TEV	*w; hspr-NLSv5TEV/HisH2AvD-mRFP1 II.2; Rad21^{ex15}, tubpr-Rad21$^{550\text{-}3TEV}$*-myc *(4c), CID-EGFP-(CGCIII.1)/ Rad21^{ex3}*
	B	-TEV	*w; +/+; Rad21^{ex15}, poliubiq-His-RFP, tubpr-Rad21$^{550\text{-}3TEV}$(4c)*
		+TEV	*w; hspr-NLSv5TEV/+; Rad21^{ex15}, poliubiq-His-RFP, tubpr-Rad21$^{550\text{-}3TEV}$(4c)/ Rad21^{ex3}*
	C		*w; hspr-NLSv5TEV/+; Rad21^{ex15}, poliubiq-His-RFP, tubpr-Rad21$^{550\text{-}3TEV}$(4c)/ Rad21^{ex3}*

S2	A,B	-TEV	*w; +/+; Rad21^{ex15}, poliubiq-His-RFP, tubpr-Rad21$^{550\text{-}3TEV}$(4c)*
		+TEV	*w; hspr-NLSv5TEV/+; Rad21^{ex15}, poliubiq-His-RFP, tubpr-Rad21$^{550\text{-}3TEV}$(4c)/ Rad21^{ex3}*
	C,D	C(2)EN	*w;C(2)EN, bw^{1},sp^{1};+/+*
S3			*w; hspr-NLSv5TEV/HisH2AvD-mRFP1 II.2; Rad21^{ex15}, tubpr-Rad21$^{550\text{-}3TEV}$*-myc *(4c), CID-EGFP-(CGCIII.1)/ Rad21^{ex3}*
S4	A	Control	*w-; HisH2AvD mRFP1 II.2 ; Rad21^{ex15}, tubpr-Rad21$^{550\text{-}3TEV}$(4c), CID-EGFP(CGC III.1)*
		+ TEV	*w-; hspr-NLSv5TEV/HisH2AvD-mRFP1 II.2; Rad21^{ex15}, tubpr-Rad21$^{550\text{-}3TEV}$*-myc *(4c), CID-EGFP-(CGCIII.1)/ Rad21^{ex3}*
		Colchicine	*w-; HisH2AvD mRFP1 II.2 ; Rad21^{ex15}, tubpr-Rad21$^{550\text{-}3TEV}$(4c), CID-EGFP(CGC III.1)*
	B, C	+ TEV	*w; +/+; Rad21^{ex15}, poliubiq-His-RFP, tubpr-Rad21$^{550\text{-}3TEV}$(4c)*
		Colchicine	*w; hspr-NLSv5TEV/+; Rad21^{ex15}, poliubiq-His-RFP, tubpr-Rad21$^{550\text{-}3TEV}$(4c)/ Rad21^{ex3}*
	D	+TEV	*w-; hspr-NLSv5TEV/Mad2-EGFP; Rad21^{ex15}, poliubiq-His-RFP, tubpr-Rad21$^{550\text{-}3TEV}$(4c)/ Rad21^{ex3}*
		Colchicine	*w-; Mad2-EGFP/CyO; Rad21^{ex15}, poliubiq-His-RFP, tubpr-Rad21$^{550\text{-}3TEV}$(4c)/TM6B*
	E	+TEV	*w-; hspr-NLSv5TEV/BubR1-EGFP; Rad21^{ex15}, poliubiq-His-RFP, tubpr-Rad21$^{550\text{-}3TEV}$(4c)/ Rad21^{ex3}*
		Colchicine	*w-; BubR1-EGFP/CyO; Rad21^{ex15}, poliubiq-His-RFP, tubpr-Rad21$^{550\text{-}3TEV}$(4c)/TM6B*
	F	+TEV	*w-; hspr-NLSv5TEV/CycB-EGFP; Rad21^{ex15}, poliubiq-His-RFP, tubpr-Rad21$^{550\text{-}3TEV}$(4c)/ Rad21^{ex3}*
		Colchicine	*w-; CycB-EGFP; Rad21^{ex15}, poliubiq-His-RFP, tubpr-Rad21$^{550\text{-}3TEV}$(4c)/TM3,Ser*

Brain Spreads and Immunofluorescence

DAPI spreads were performed by dissecting brains in 0.7% NaCl and incubated for 2 min in 45% acetic acid. Brains were transferred to a siliconized coverslip with 5 µl of 60% acetic acid for 30 seconds, squashed and transferred to liquid nitrogen. Slides were allowed to air dry before mounting in Vectashield mounting medium containing DAPI. For immunofluorescence, brains were dissected in 0.7% NaCl, incubated with 100 µM colchicine for one hour (when indicated), hypotonic shocked in 0.5% sodium citrate for 2–3 minutes, and fixed on a 5 µl drop of fixative (3.7% formaldehyde, 0.1% Triton-X100 in PBS) placed on top of a siliconized coverslip. After 30 seconds, the brains were squashed between the coverslip and a slide, allowed to fix for an additional 1 min and then placed in liquid nitrogen. Slides were further extracted with 0.1% Triton-X100 in PBS for 10 min, and proceded for immunofluorescence following standard protocols. Primary antibodies were rat anti-CID (Martins et al., 2009) used at 1:2000, rabbit anti-Mad1 used at 1:2000 (Conde et al., 2013), rabbit anti-BubR1 used at 1:2000 (Logarinho et al., 2004), anti-Aurora B rabbit used at 1:2000 (Adams et al., 2001), anti H3T3ph rabbit used at 1:1000 (Active Motif). Secondary antibodies conjugated with fluorescent dyes from Alexa series (Invitrogen) were used according to the manufacturer's instructions. All the fixed samples were observed with an inverted wide-field DeltaVision microscope (Applied Precision Inc.) equipped with a 10061.4 oil immersion objective (Olympus) and an EMCCD camera (Roper Cascade II or Roper Cascade 1024).

Tissue Preparation for live cell imaging

For live imaging brains were dissected 30 minutes after heat-shock in Schneider medium supplemented with 10% FBS (plus 100 µM Colchicine (Sigma), when indicated). Brains were mounted in 8 µl of medium in 35mm glass bottom dishes (MatTek), covered with an oxygen-permeable membrane (YSI membrane kit), and sealed with Voltalef 10S oil (VWR). This procedure allowed for long-term live imaging of 4-8 hours. For experiments that included drug addition during imaging acquisition (Binucleine 2 (Sigma-Aldrich) to a final

concentration of 25 µM and Roscovitine (Sigma-Aldrich) to the indicated final concentrations), brains were mounted in 200 µl of medium in the 35mm glass bottom dish coated by Concanavalin A. For characterization of the attachment profile upon cohesion depletion, brains were dissected in Schneider medium containing 10% FBS and 1:10 000 Sir Tubulin probe (Spirochrome). Given the low permeability of intact brains to the probe, the sample was cut into pieces and allowed to incubate for 30 minutes. Brains were subsequently squashed between the slide and a coverslip by capillary forces as previously described (Buffin et al., 2005). Time-lapse microscopy was performed with a spinning disk confocal microscope (Andor Revolution XD system) equipped with a 60xOil objective (Nikon, NA 1.4) and an Andor iXon 897 camera was used. All images were acquired by using a 20-26 µm thick imaging plane with 1 µm incremental z steps (except for chromosome attachment profiling where 0.2 was used). All images were assembled using ImageJ software (http://rsb.info.nih.gov/ij/) and selected stills were processed with Photoshop.

Measurements

All quantifications were performed using ImageJ software. Image z-stacks were projected (maximum projection) and background subtracted. For quantification of Aurora B and H3T3ph levels at the kinetochore, a fixed size ROI was used (1.6 x 0,5 µm in control chromosomes and 0.8 x 0,5 µm in single sisters). This ROI was placed between the kinetochore(s) and the centromeric signal and mean fluorescence intensity of AurB/H3T3Ph was normalized to corresponding CID. For measurements of kinetochore motion, CID-EGFP was imaged at 1-minute intervals. Images were segmented to select the centromere regions, based on a manual threshold (set 8 min post NEBD), to create binary images. For each movie, a walking average of 3 frames was produced (using kymograph plug-in, written by J. Rietdorf and A. Seitz, EMBL, Heidelberg, Germany) creating a merged image in which the intensity is proportional to the overlap between consecutive frames. Intensity profiles were used to estimate the percentage of non-overlaping, 2-frame overlap and 3-frame overlap pixels. Motion was quantified from the timeframe at which centromeres reached the poles (6-10 min post NEBD) until anaphase onset. Attachment profiles were scored based on CID-EFGP signal interactions with the microtubules labeled by SIR tubulin (1:10 000). Images were taken with a short z-distance (0,2 µm) and the attachment state of each kinetochore was scored in 3D by observing the entire z stack. Attachments were considered end-on if a single k-fiber was observed protruding from the centromere, lateral if the centromere was placed adjacently to a defined MT-fiber, merotelic if two fibers from opposite poles could be detected on a single centromere and unattached if CID-labelled centromeres were devoid of any MT fibers in their vicinity.

For measurement of Mad2, BubR1 and Cyclin B kinetics, brains were imaged in a 2 minutes interval (except for long-term CycB imaging were images were taken every 10 min). For analysis of Mad2 and BubR1 levels, a manual threshold was set to select the kinetochores 8 min after NEBD. Relative fluorescence was calculated by multiplying the area above the threshold by the mean fluorescence intensity, divided by the

maximal value within each dataset. For Cyclin B measurements, an ROI that comprises the entire NBs was used. Mean fluorescence intensities were measured at each time point and background subtracted (mean fluorescence intensity 4 minutes after anaphase onset). Relative fluorescence intensities were calculated by dividing by the maximum intensity within each data set.

Statistic analysis.

Statistical comparisons between sets of data were done using One-way or Two-way ANOVA (for multiple comparisons). All the statistic evaluation and graphic work was done in Graph Pad Prism 5. For each experimental set, “n” refers to the number of cells/kinetochores evaluated and “N” to the number of independent brains.

Mathematical modelling

The error-correction (EC) and Spindle Assembly Checkpoint (SAC) modules (Fig. 4) were converted into reaction-rate equations based on the following assumptions. The "Basic" and the "SAC-feedback" models are simplified versions of the "SAC-EC-feedback model", hence the description is based on the later and the changes to the simpler models are highlighted.

AurB molecules ($AurB_T$) are distributed between the centromeric form ($AurB_c$) and other cellular compartments ($AurB_T$ – $AurB_c$). In general, the models describe the localization of AurB at centromeres ($AurB_c$) as a combination of Cdk1:CycB-independent (k_{loc}) and -dependent (k_{loc_cdk}) processes. $AurB_c$ dissociation from centromeres follows first order kinetics with a rate constant of k_{rem} =2.5 min^{-1} and k_{rem} =10 min^{-1} in the presence and in the absence of cohesins, respectively:

$$\frac{d[AurB]_c}{dt} = \left(k_{loc} + k_{loc,cdk} \cdot [Cdk1]\right) \cdot ([AurB]_T - [AurB]_c) - k_{rem} \cdot [AurB]_c$$

The kinetic parameters of AurB localization are summarized below:

	"Basic model"	"SAC-feedback model"	"SAC-EC-feedback model"
k_{loc} (min^{-1})	3	3	0
$k_{loc,cdk}$ (min^{-1})	0	0	5

In case of Cdk1-driven localization ("SAC-EC-feedback model"), the steady state fraction of AurB at centromeres during prophase (Cdk1 = 1) is given by $\frac{[AurB]_c}{[AurB]_T} = \frac{k_{loc,cdk} \cdot [Cdk1]}{k_{loc,cdk} \cdot [Cdk1] + k_{rem}}$, which is 0.666 and 0.333 in the presence and in the absence of cohesins, respectively. We choose the total level of AurB 1.5 a.u., which sets the level of the centromeric pool ($AurB_c$) to 1 a.u. at the beginning of normal mitosis. Only a fraction of centromeric AurB ($AurB_a$) can destabilize MT-KT attachments at kinetochores (attached Microtubule Binding Sites - aMBS), because of kinetochore stretching caused by spindle tension. The rate of MT-KT attachments is proportional to MT-density (MT) and number of unattached MT binding sites at KTs (MBS_T - aMBS):

$$\frac{d[aMBS]}{dt} = k'_{att} \cdot [MT] \cdot ([MBS]_T - [aMBS]) - k_{err} \cdot \frac{[AurB]_a}{1 + [BN2]} \cdot [aMBS]$$

where [BN2] corresponds to the concentration of AurB inhibitor (binuclein2) relative to its IC_{50} value. Using 20-fold AurB inhibition ([BN2]=19) in the "SAC-EC-feedback model" reduces the length of TEV-induced mitosis (~45 mins) to about 9 mins (simulation not shown), consistent with our experiments on Fig. 2E.

The 'active' form of AurB ($AurB_a$) is reduced by MT-KT attachments (aMBS) according to a Hill-function (Ferrell and Ha, 2014), which approximates the cooperative effects among attached MT binding sites:

$$[AurB]_a = [AurB]_c \cdot \left(1 - Stretch \cdot \frac{[aMBS]^N}{J^N + [aMBS]^N}\right)$$

The value of Stretch parameter is one for chromosomes (Xs) and much smaller than one for individual sister-chromatids (SCs). Similar values were chosen for rate constants of MT-KT attachments (k_{att} =0.5 min^{-1}) and detachments (k_{err} =0.66 min^{-1}) which guarantees that saturating KTs with MT attachments requires AurB inactivation by the Stretch. In order to simulate the effect of spindle disruption by colchicine, MT should be set to zero.

The cellular level of APC/C is assumed to be constant (APC_T = 1 a.u.) during mitosis and distributed between active, free (APC) and MCC-bound, inactive (APC_T – APC) forms. The level of active APC is decreased by rapid MCC binding and increased by dissociation and disassembly of MCC (He et al., 2011):

$$\frac{d[APC]}{dt} = (k_{diss} + k_{imcc}) \cdot ([APC]_T - [APC]) - k_{ass} \cdot [APC] \cdot [MCC]_{free}$$

Association (k_{ass} = 200 min^{-1}) and dissociation (k_{diss} = 0.01 min^{-1}) rate constants are chosen to describe a tight binding of MMC and APC/C (Hein and Nilsson, 2014). The level of the limiting MCC component (labelled by MCC_T) is assumed to be in excess over APC/C (MCC_T =1.2 > APC_T), which is necessary requirement for stoichiometric inhibition (Verdugo et al., 2013). The assembled MCC could be associated with APC/C (APC_T – APC) or present in a free form (MCC_{free}). MCC_{free} is produced by unattached KTs from the pool of free MCC subunits at a rate proportional to the level of the limiting component (MCC_T – MCC_{free} - APC_T + APC). In the two models with SAC-feedbacks, the rate of production of MCC_{free} is proportional to both $AurB_a$ and Cdk1 activities, because these kinases activate checkpoint proteins at the kinetochore. The level of MCC_{free} is decreased by binding to APC/C (k_{ass}) and by disassembly of the complex (k_{imcc} = 0.5 min^{-1}) and it increased by dissociation from the MCC:APC complex (k_{diss}):

$$\frac{d[MCC]_{free}}{dt} = \left(k_{amcc} + k_{amcc,kin} \cdot \frac{[AurB]_a/(1+[BN2])}{J_{amc} + [AurB]_a/(1+[BN2])} \cdot [Cdk1]\right) \cdot [uMBS]$$
$$\cdot \left([MCC]_T - [MCC]_{free} - ([APC]_T - [APC])\right) - k_{ass} \cdot [APC] \cdot [MCC]_{free} + k_{diss}$$
$$\cdot ([APC]_T - [APC]) - k_{imcc} \cdot [MCC]_{free}$$

The kinetic parameters of MCC production are summarized below:

	"Basic model"	"SAC-feedback model"	"SAC-EC-feedback model"
k_{amcc} (min^{-1})	10	0	0
$k_{amcc\_,cdk}$ (min^{-1})	0	15	15

The low sensitivity of SAC to AurB inhibition (our data and (Santaguida et al., 2011)) suggests an efficient activation of SAC-proteins by AurB–kinase, which we describe with a hyperbolic ('saturating') function using a small 'saturation-constant' (J_{amc} = 0.1). Therefore after a 20-fold ([BN2]=19) inhibition the residual 5% activity of AurB-kinase could maintain a third of the MCC production rate. These parameter values reduce the length of colchicine-induced mitotic arrest, upon AuroraB inhibition, to about 60 mins (simulation not shown) in the "SAC-EC-feedback model", consistent with our experiments on Fig. 2E.

CycB is synthesized at a constant rate (k_{scycb}) and associates rapidly with Cdk1 present in excess, therefore the level of CycB determines Cdk1 activity via

$$[Cdk1] = \frac{[CycB]}{1 + [RO]}$$

where [RO] corresponds to the concentration of Cdk-inhibitor (roscovitine) relative to its IC_{50} value.

Cdk1 is inactivated by CycB degradation which has a small, APC/C-independent (k_{dcycb} = 0.004 min^{-1}, $t_{½}$ ≅ 170 min) and a large, APC/C-dependent rate constants ($k_{dcycb,apc}$ = 0.5 min^{-1} = $t_{½}$ ≅ 1.4 min):

$$\frac{d[CycB]}{dt} = k_{scycb} - \left(k_{dcycb} + k_{dcycb,apc} \cdot [APC]\right) \cdot [CycB]$$

The steady state level of CycB in the absence of APC/C activity (interphase) is k_{scycb}/k_{dcycb}, which we set to one by choosing the rate of CycB synthesis (k_{scycb}) identical to k_{dcycb} (= k_{scycb} = 0.004 min^{-1}).

The model was simulated by Gillespie's Stochastic Simulation Algorithm (SSA) after converting the rate of elementary reactions into propensity functions. We provide the code for stochastic simulation in the form of an ode-file for the freely available software XPPAut (http://www.math.pitt.edu/~bard/xpp/xpp.html).

To run the simulations in a programmatical manner, we used an scripting-interface for XPPAut (https://github.com/novakgroupoxford/XPPjl). The original code used to run and plot the simulations used in the figures is freely available at https://github.com/novakgroupoxford/2015_Mirkovic_et_al.

The initial conditions of numerical simulations are obtained from a steady state calculated without MT-binding to KTs (MT= 0) and lack of APC/C activity (k_{dcycb_apc} = 0), which corresponds to an interphase situation. The start of numerical simulations corresponds to nuclear envelope breakdown when the mitotic spindle starts to capture kinetochores and APC/C is activated by Cdk1:CycB, which is captured by setting [MT]= 1 and $k_{dcycb,apc}$ = 0.5 min^{-1}.

The stochastic simulation follows the number of molecules in a total volume (V_T) of 10^4 units. V_T is divided into a smaller (V_x) and a larger (V_{nx}) compartment in order to follow a single sister-kinetochore of a chromosome (normal mitosis)/sister-chromatid (TEV induced mitosis) and the collection of all the kinetochores within the cell, respectively. Since Drosophila somatic cells have 16 sister-kinetochores, the small volume is $V_x = V_T/16 = 625$ units while $V_{nx} = 15V_T/16 = 9375$. The components of the SAC (cytoplasmic) module are assumed to be more abundant than the EC (kinetochore/centromere) ones. Since we set the level of APC_T = 1and MCC_T = 1.2, these molecules are represented in the volume of 10^4 by 10^4 and $1.2 \cdot 10^4$ copies, respectively. The choice of $k_{scycb} = k_{dcycb}$ sets the initial number of CycB molecules to 10^4. Zero- and second-order rate-constants of the deterministic (concentration) models were scaled by volume and relative protein abundance.

We assume 11 microtubule-binding sites (MBS) on each sister-kinetochore (Maiato et al., 2006), which gives 176 binding sites on 16 sister-kinetochores, therefore we set the parameter MBS_{tot} = 0.0176. By choosing $AurB_T$ = 0.15 the total number of Aurora B molecules is $1.5 \cdot 10^3$, which are distributed between centromeric and free pools. At the beginning of mitosis, two-third (~10^3) and one-third (~500) AurB molecules are bound to centromeres in the presence and in the absence of cohesins, respectively (see above). These centromeric AurB molecules are distributed randomly among eight chromosomes and 16 sister-chromatids. Therefore on average ~60 (=1000/16) and ~30 (=500/16) AurB molecules are acting on a single sister-kinetochore in the presence and in the absence of cohesins, respectively.

```
##################################################
#
#      FULL STOCHASTIC MODEL FOR MIRKOVIC ET AL. 2015
#
##################################################

##################################################
#
#      VARIABLES
#
##################################################

# time for next reaction
tr'=tr-log(ran(1))/p14
uKT'=max(0,uKT+z1-z2)
APC'=max(1,APC+z3-z4)
MCCfree'=max(1,MCCfree+z5-z6)
CycB'=max(1,CycB+z7-z8)
AurBc'=max(0,AurBc+z9-z10)
uKTla'=max(0,uKTla+z11-z12)
AurBcla'=max(0,AurBcla+z13-z14)

##################################################
#
#      REACTION RATES
#
##################################################

# formation of unattached MT binding sites at the kinetochore of a single chromosome/sister-chromatid
V1 = kerr*AurBa/(1 + BN2)*(KTtot*Vx - uKT)/Vx
# formation of unattached MT binding sites at the kinetochore of a single chromosome/sister-chromatid
V2 = katt*uKT

# APC/C activation
V3 = (kdiss + kimcc)*(APCtot*VT - APC)
# APC/C inactivation
V4 = kass*APC*MCCfree/VT

# MCC production
V5 = (kamcc + kamcc_cdk/VT*Cdk1*AurBatot/(1 + BN2)/(Jamcc + AurBatot/(1 + BN2)))*(uKT + uKTla)*(MCCtot*VT - MCCfree - (APCtot*VT - APC))/VT + kdiss*(APCtot*VT
- APC)
# MCC inactivation
V6 = kimcc*MCCfree + kass*APC*MCCfree/VT

# CycB synthesis
V7 = kscycb*VT
# CycB degradation
V8 = (kdcycb + kdcycb_c*APC/VT)*CycB

# Aurora-B association with the centromere of a single chromsome/sister-chromatids
V9 = (kloc + kloc_cdk/VT*Cdk1)*(AurBtot*VT - AurBc - AurBcla)*Vx/VT
# Aurora-B dissociation form centromere of a single chromosome/sister-chromatids
V10 = krem*AurBc

# formation of unattached kinetochores of bulk chromosomes/sister-chromatids
V11 = kerr*AurBala/(1 + BN2)*(KTtot*Vbulk - uKTla)/Vbulk
# formation of attached kinetochores of bulk chromosomes/sister-chromatids
V12 = katt*uKTla

# Aurora-B association with the centromere of bulk chromsome/sister-chromatids
V13 = (kloc + kloc_cdk/VT*Cdk1)*(AurBtot*VT - AurBcla - AurBc)*Vbulk/VT
# Aurora-B dissociation form centromere of bulk chromosome/sister-chromatids
V14 = krem*AurBcla

##################################################
#
#      CUMULATIVE PROBABILITIES
#
##################################################

p1 = V1
p[2..14] = p[j-1] + V[j]

##################################################
#
#      CHOOSE REACTION
#
##################################################

s2 = ran(1)*p14
z1 = (s2<p1)
z[2..13]=(s2<p[j])&(s2>=p[j-1])
z14 = (s2>p13)
```

```
################################################
#
#      ALGEBRAIC EQUATIONS AND AUXILLIARY VARIABLES
#
################################################

AurBa=flr(AurBc*(1 - Stretch*(KTtot*Vx - uKT)^N/((J*KTtot*Vx)^N + (KTtot*Vx - uKT)^N)))
AurBala=flr(AurBcla*(1 - Stretch*(KTtot*Vbulk - uKTla)^N/((J*KTtot*Vbulk)^N + (KTtot*Vbulk- uKTla)^N)))
AurBatot=AurBa + AurBala
Cdk1=CycB/(1 + RO)
VT=Vx + Vbulk

aux uKTtot=uKT + uKTla
aux AurBa=AurBa
aux AurBctot=AurBc + AurBcla
aux AurBatot=AurBa + AurBala



################################################
#
#      INITIAL CONDITIONS
#
################################################

init tr=0
init uKT=11
init APC=117
init MCCfree=2128
init CycB=10052
init AurBc=62
init uKTla=165
init AurBcla=938

################################################
#
#      PARAMETERS
#
################################################

p Vx=625
p Vbulk=9375

p kass=200
p kdiss=0.01
p BN2=0
p RO=0
p kerr=6.66
p katt=0.5
p KTtot=0.0176
p N=4
p J=0.4
p Jamcc=50
p kamcc=0
p kamcc_cdk=750
p kimcc=0.5
p MCCtot=1.2
p kscycb=0.004
p kdcycb=0.004
p kdcycb_c=0.5
p kloc=0
p kloc_cdk=5
p krem=2.5
p Stretch=1
p APCtot=1
p AurBtot=0.15


################################################
#
#      NUMERICAL SETTINGS
#
################################################

@ bound=100000000
@ meth=discrete
@ total=2000000
@ njmp=1000
@ maxstorage=100000000
@ seed=189284124
done
```

SUPPLEMENTAL REFERENCES

Adams, R.R., Maiato, H., Earnshaw, W.C., and Carmena, M. (2001). Essential roles of Drosophila inner centromere protein (INCENP) and aurora B in histone H3 phosphorylation, metaphase chromosome alignment, kinetochore disjunction, and chromosome segregation. The Journal of cell biology *153*, 865-880.

Conde, C., Osswald, M., Barbosa, J., Moutinho-Santos, T., Pinheiro, D., Guimaraes, S., Matos, I., Maiato, H., and Sunkel, C.E. (2013). Drosophila Polo regulates the spindle assembly checkpoint through Mps1-dependent BubR1 phosphorylation. The EMBO journal *32*, 1761-1777.

Ferrell, J.E., Jr., and Ha, S.H. (2014). Ultrasensitivity part I: Michaelian responses and zero-order ultrasensitivity. Trends in biochemical sciences *39*, 496-503.

He, E., Kapuy, O., Oliveira, R.A., Uhlmann, F., Tyson, J.J., and Novak, B. (2011). System-level feedbacks make the anaphase switch irreversible. Proceedings of the National Academy of Sciences of the United States of America *108*, 10016-10021.

Hein, J.B., and Nilsson, J. (2014). Stable MCC binding to the APC/C is required for a functional spindle assembly checkpoint. EMBO reports *15*, 264-272.

Huang, J., and Raff, J.W. (1999). The disappearance of cyclin B at the end of mitosis is regulated spatially in Drosophila cells. The EMBO journal *18*, 2184-2195.

Maiato, H., Hergert, P.J., Moutinho-Pereira, S., Dong, Y., Vandenbeldt, K.J., Rieder, C.L., and McEwen, B.F. (2006). The ultrastructure of the kinetochore and kinetochore fiber in Drosophila somatic cells. Chromosoma *115*, 469-480.

Martins, T., Maia, A.F., Steffensen, S., and Sunkel, C.E. (2009). Sgt1, a co-chaperone of Hsp90 stabilizes Polo and is required for centrosome organization. The EMBO journal *28*, 234-247.

Novitski, E., Grace, D., and Strommen, C. (1981). The entire compound autosomes of Drosophila melanogaster. Genetics *98*, 257-273.

Schuh, M., Lehner, C.F., and Heidmann, S. (2007). Incorporation of Drosophila CID/CENP-A and CENP-C into Centromeres during Early Embryonic Anaphase. Current biology : CB *17*, 237-243.

Verdugo, A., Vinod, P.K., Tyson, J.J., and Novak, B. (2013). Molecular mechanisms creating bistable switches at cell cycle transitions. Open biology *3*, 120179.